International Journal of Nanomedicine

Dovepress

open access to scientific and medical research

Open Access Full Text Article

ORIGINAL RESEARCH

Enzyme-Linked Lipid Nanocarriers for Coping Pseudomonal Pulmonary Infection. Would Nanocarriers Complement Biofilm Disruption or Pave Its Road?

Noha Nafee[1,2], Dina M Gaber[3], Alaa Abouelfetouh[4,5], Mustafa Alseqely[4], Martin Empting[6], Marc Schneider[7]

[1]Department of Pharmaceutics, College of Pharmacy, Kuwait University, Safat, 13110, Kuwait; [2]Department of Pharmaceutics, Faculty of Pharmacy, Alexandria University, Alexandria, 21521, Egypt; [3]Department of Pharmaceutics, Division of Pharmaceutical Sciences, College of Pharmacy, Arab Academy for Science, Technology and Maritime Transport, Alexandria, 1029, Egypt; [4]Department of Microbiology and Immunology, Faculty of Pharmacy, Alexandria University, Alexandria, 21521, Egypt; [5]Department of Microbiology and Immunology, Faculty of Pharmacy, Alamein International University, Alamein, 5060335, Egypt; [6]Helmholtz-Institute for Pharmaceutical Research Saarland (HIPS), Department of Antiviral and Antivirulence Drugs (AVID), Saarland University, Saarbrücken, 66123, Germany; [7]Department of Pharmacy, Biopharmaceutics and Pharmaceutical Technology, Saarland University, Saarbrücken, 66123, Germany

Correspondence: Noha Nafee, Department of Pharmaceutics, College of Pharmacy, Kuwait University, Safat, 13110, Kuwait, Tel +96524634914; +96560300583, Fax +96524636843, Email noha.nafee@ku.edu.kw

Introduction: Cystic fibrosis (CF) is associated with pulmonary *Pseudomonas aeruginosa* infections persistent to antibiotics.

Methods: To eradicate *pseudomonal* biofilms, solid lipid nanoparticles (SLNs) loaded with quorum-sensing-inhibitor (QSI, disrupting bacterial crosstalk), coated with chitosan (CS, improving internalization) and immobilized with alginate lyase (AL, destroying alginate biofilms) were developed.

Results: SLNs (140–205 nm) showed prolonged release of QSI with no sign of acute toxicity to A549 and Calu-3 cells. The CS coating improved uptake, whereas immobilized-AL ensured >1.5-fold higher uptake and doubled SLN diffusion across the artificial biofilm sputum model. Respirable microparticles comprising SLNs in carbohydrate matrix elicited aerodynamic diameters MMAD (3.54, 2.48 µm) and fine-particle-fraction FPF (65, 48%) for anionic and cationic SLNs, respectively. The antimicrobial and/or antibiofilm activity of SLNs was explored in *Pseudomonas aeruginosa* reference mucoid/nonmucoid strains as well as clinical isolates. The full growth inhibition of planktonic bacteria was dependent on SLN type, concentration, growth medium, and strain. OD measurements and live/dead staining proved that anionic SLNs efficiently ceased biofilm formation and eradicated established biofilms, whereas cationic SLNs unexpectedly promoted biofilm progression. AL immobilization increased biofilm vulnerability; instead, CS coating increased biofilm formation confirmed by 3D-time lapse confocal imaging. Incubation of SLNs with mature biofilms of *P. aeruginosa* isolates increased biofilm density by an average of 1.5-fold. CLSM further confirmed the binding and uptake of the labeled SLNs in *P. aeruginosa* biofilms. Considerable uptake of CS-coated SLNs in non-mucoid strains could be observed presumably due to interaction of chitosan with LPS glycolipids in the outer cell membrane of *P. aeruginosa*.

Conclusion: The biofilm-destructive potential of QSI/SLNs/AL inhalation is promising for site-specific biofilm-targeted interventional CF therapy. Nevertheless, the intrinsic/extrinsic fundamentals of nanocarrier–biofilm interactions require further investigation.

Keywords: alginate lyase, chitosan, solid lipid nanoparticles, cystic fibrosis, *Pseudomonas aeruginosa*, quorum-sensing inhibitors

Introduction

Around 75% of adult cystic fibrosis (CF) patients suffer from the invasion of mucoid, alginate-producing strains of *Pseudomonas aeruginosa* that wreaks havoc upon the airways leading to accelerated deterioration of pulmonary function and ending in substantial morbidity.[1] The mucoid phenotype of *P. aeruginosa* – being pathognomonic for the disease – poses multiple challenges to effective treatment. Pathogenicity traits allowing *P. aeruginosa* to endure, proliferate, and profoundly

Received: 17 November 2023
Accepted: 28 March 2024
Published: 29 April 2024

affect all stages of CF pulmonary disease can be predicated by multiple virulence factors and biofilm formation. In addition to the mechanical stability of mature *P. aeruginosa* biofilms persisting in the respiratory tract, alginate overproduction is involved in the establishment of microcolonies at the beginning of biofilm formation, in addition to mechanical stability of mature *P. aeruginosa* biofilms persisting in the respiratory tract. *P. aeruginosa* biofilm is a self-produced matrix of polysaccharides (eg, alginate), proteins, nucleic acids and lipids forming a three-dimensional network responsible for interconnection of a core of inactive "persister" cells and mediating biofilm adherence to surfaces, gel formation and mechanical stability.[2] These nonmotile polymicrobial aggregates − elsewhere referred to as "capsulated *P. aeruginosa*" – are less sensitive to host defenses and possess up to 1000-fold increased tolerance toward antipseudomonal drugs, thus, herald deleterious effects on CF lung.[3]

Alginate (a high-molecular-mass exopolysaccharide, unbranched heteropolymer) consists of 1,4-linked uronic residues, β-d-mannuronate (M) and α-l-guluronate (G). These components are arranged in homopolymeric blocks of polymannuronate and heteropolymeric sequences with a random distribution of guluronate and partially O-acetylated mannuronate residues.[2] As a key component of *P. aeruginosa* biofilm, alginate plays a key pathogenic role through interrupting the phagocytosis of macrophages and neutrophils, restricting lymphocyte function, and inducing inflammatory reactions, thus, aggravating lung infection.[1,4] Specifically, O-acetylation of the M residues at the C2 and/or C3 positions of alginate synthesized by *P. aeruginosa* ameliorates alginate resistance toward degradation, triggering serious resistance of *P. aeruginosa* to phagocytic cells and even to aggressive antibiotic regimen.[5]

Owing to the complexity of the biofilm matrix, the complete degradation of all components compels a range of enzymes, alginate lyase (AL). AL is reported to degrade alginate by cleaving the glycosidic bond via a beta-elimination reaction, yielding oligomers with 4-deoxy-L-erythro-hex-4-enepyranosyluronate at the nonreducing end.[6] AL can be classified as endo- and exo-type lyases according to the mode of the cleavage site, where they commonly possess endo-type lyase activity. Currently, most AL ensure poly M-specific lyase activity, preferably by degrading the poly M-alginate block.[6] Reduced alginate levels consequently increase the innate immune response and promote phagocytosis.

Several strategies have been developed to eradicate *P. aeruginosa* biofilms and overcome antibiotic resistance to manage lung infections in CF patients. In the last 25 years, antibiotics have been encapsulated into micelles, liposomes,[3,7] chitosan nanoparticles (CS NPs),[8,9] PLGA NPs[10] and lipid nanocapsules.[11] Despite the progress of antibiotic-loaded nanoparticles, broad biofilm eradication could not be achieved presumably due to low antibiotic exposure in the vicinity of *P. aeruginosa* biofilms.[12] Alipour et al[13] evidenced that liposomal aminoglycosides (tobramycin, gentamicin and amikacin) did not fare better antipseudomonal activity than conventional forms against *P. aeruginosa* in CF sputum; the latter overwhelmingly blocked the transport of the nanosystems.[7] Some studies even reported (2–8-fold) lower activity of liposomal than free antibiotics. This has led to the development of adjuvant therapeutic agents that can act alongside conventional antibiotics, thereby potentiating their action.

Understanding the host–pathogen interface elucidates the adaptive mechanisms empowering *P. aeruginosa* evasion of host immunity and spurs the development of novel therapeutics. To date, innovative approaches include the disruption of the DNA−Ca^{2+}−DNA bridges of *P. aeruginosa* biofilms using lytic enzymes such as recombinant human deoxyribonuclease (rhDNase) to cleave DNA and decrease sputum viscosity, the use of lectin inhibitors to control bacterial adhesion and biofilm formation, in addition to bacteriophages targeting the *Pseudomonas* genus, quorum-sensing inhibitors (QSI), and antimicrobial peptides.[14–18] Reported challenges for these strategies include poor stability, proteolytic sensitivity, immunogenicity, hemolytic activity, bacterial resistance, and high cost.[9]

P. aeruginosa regulates much of its virulence via quorum-sensing (QS), a mechanism by which individual bacteria communicate with each other through the production and detection of small signal molecules.[19,20] *P. aeruginosa* produces *Pseudomonas* quinolone signal (PQS), which activates PqsR (also referred to as a multiple virulence factor regulator), which drives the coordinated expression of nearly 200 genes related to virulence factors. Based on the fact that PQS is overproduced in CF sputum, blocking the PQS-QS system or "quorum-quenching" should make *P. aeruginosa* lung infection in CF patients better treatable. Our collaborators demonstrated the potential of various PqsR antagonists as QSI for disrupting cell-to-cell communication and biofilm formation.[21–25] Yet, reduction of mucociliary clearance, together with *P. aeruginosa* biofilm colonization, guard the cargo against reaching its site of action. Impaired penetration could be overcome via mucus-penetrating solid lipid nanoparticles (SLNs), which ensured

up to 7-fold superior anti-virulence activity relative to free QSI.[26] Moreover, combination of QSI with tobramycin in self-assembled squalenyl NPs demonstrated a significant synergistic effect.[24]

In line with that, chitosan proved potential antimicrobial and biofilm-disrupting activity.[27] The electrostatic interactions of the cationic CS with anionic phospholipids on the bacterial cell membrane, lipopolysaccharides on the cell wall of Gram negative bacteria and/or teichoic acids in Gram positive bacteria, destabilize the cell envelope.[27] Coating the surface of SLNs with CS was thus expected to ameliorate the outcome of the system.

An emerging therapeutic approach encompasses the use of AL to destroy alginate with the aim of effectively dispersing biofilm architecture, thus enabling better antibiotic penetration.[13] A promising protocol involves the co-administration of AL with antibiotics to increase bacterial sensitivity towards antimicrobials. Studies proved potential elimination of mucoid bacteria using either gentamicin or ceftazidime with AL[28] and applying AL to aminoglycoside antibiotics limited *P. aeruginosa* biofilm growth and bacterial count in CF sputum.[13] Being a biodegradable enzyme, negligible hazards can be speculated. Owing to AL poor thermal stability,[9] strategies to stabilize the enzyme included introduction of a disulfide bond[29] and the use of glycerol as stabilizer.[30] Immobilization of AL onto/into NPs was recently introduced to shield against thermal damage. Nanocomposites containing ceftazidime-, AL-loaded silver NPs and thioether-bridged mesoporous organosilica exhibited strong growth inhibition of PAO1 strain and biofilm degradation.[31] In parallel, ciprofloxacin-loaded CS-NPs functionalized with AL reduced biofilm thickness, biomass and density.[8]

Herein, to bolster the rationale of the QSI-loaded SLNs therapeutic approach, the particles were surface-functionalized with AL and CS coatings. SLNs were then spray-dried to obtain respirable microparticles. Following physicochemical characterization, penetration of the artificial biofilm sputum medium, viability, and uptake in pulmonary cell lines were investigated. The potential of SLNs bearing biofilm-degrading enzyme functionalities to kill *P. aeruginosa*, prohibit biofilm formation, or disassemble the biofilm matrix was assessed in reference strains and clinical isolates.

Materials and Methods

Materials

The quorum-sensing inhibitor (QSI) used in this study was previously reported as compound 3 by Lu et al.[23] It is an alkylquinolone-derived inverse agonist of the QS receptor PqsR with the IUPAC name 2-heptyl-6-nitro-4-oxo-1,4-dihydroquinoline-3-carboxamide and has been synthesized and characterized according to previously reported procedures.[23,32] Gelucire (43/01) was donated by Gattefossé, Saint Priest, France. Poloxamer 407 (PX) was obtained from BASF (Germany). Low molecular weight ultrapure chitosan chloride (Protasan UP CL 113) and sodium alginate (Pronova ultrapure alginate MVM, <75 kDa, intermediate viscosity >200 mPa*s) were purchased from (Novamatrix, FMC, Sandvika, Norway). Hydroxyethyl cellulose 250M (HEC) was obtained from SE Tylose GmbH & Co.KG, Wiesbaden, Germany). Alginate lyase, coumarin-6 (cou), Calcofluor-White, MTT, 3-(4,5-dimethylthiazol-2-yl)-2,5-diphenyltetrazolium bromide, mucin from porcine stomach type II, DNA (low molecular weight from salmon sperm), Trizma base, sodium chloride, potassium chloride, 4′,6-diamidino-2-phenylindole (DAPI), and diethylenetriaminepentaacetic acid (DTPA) were purchased from Sigma–Aldrich (Steinheim, Germany). Egg yolk emulsion was obtained from Oxoid Ltd (Hampshire, UK). Bacto Casamino acid was purchased from Difco Laboratories Becton Franklin Lakes, NJ, USA). Alexa Fluor 633 wheat germ agglutinin (WGA) was obtained from Invitrogen (Carlsbad, USA. The live/dead BacLight Bacterial Viability Kit was purchased from Molecular Probes Inc. (Oregon, USA). All other reagents and solvents used were of analytical grade.

Methods

Preparation and Characterization of SLNs

SLNs were prepared via a hot homogenization technique using Gelucire 43/1 as a lipid and poloxamer 407 as a stabilizer, as detailed in the Supplementary Materials. Positively charged particles were prepared by adding chitosan (0.05% w/v) to PX solution prior to particle preparation. The selected SLNs were loaded with QSI (50 µg/mL SLNs). For the uptake and biofilm penetration studies, the QSI was substituted with coumarin-6 (30 µg/mL SLNs).

AL-modified SLNs were obtained by adding an aqueous AL solution to a preformulated SLN dispersion (25 U/mL SLNs). Table 1 lists the different SLN formulations used in this study.

SLNs were characterized in terms of size, polydispersity index (PdI) and ζ-potential in addition to morphological examination by TEM, yield, and pH measurements. Thermal properties were investigated by DSC, and surface functionalization with alginate lyase was verified by Fourier-transform infrared (FT-IR) spectroscopy. The experiments are described in the Supplementary Materials.

Entrapment of QSI and in vitro Release

QSI-loaded SLNs were purified by centrifugal ultrafiltration using Centrisart-I® (MWCO 10 kDa, Sartorius AG, Goettingen, Germany) to get rid of free QSI. The concentration of QSI entrapped in SLNs was quantified by liquid chromatography coupled with tandem mass spectrometry (LC-MS/MS), as previously described.[26] The entrapment efficiency (EE) and loading efficiency (LE) of QSI were determined after payload extraction from purified loaded particles in methanol/dichloromethane.

The release of QSI from SLNs was investigated in 50 mL simulated lung fluid (SLF; pH 7.4) at physiological temperature for 24 h, as described in the Supplementary Materials. The release profiles were fitted to different kinetic models to determine the relevant release mechanisms.

Cell Viability (MTT Assay)

The effects of different concentrations of plain and QSI-loaded SLNs (±CS, ±AL) on human alveolar lung carcinoma, A549 (CCL-185; ATCC, Manassas, VA, USA), and bronchial Calu-3 (HTB-55; ATCC, Manassas, VA, USA) cell lines were investigated using an MTT viability assay (Supplementary Materials). Cytotoxic concentrations (CC_{50}) of the tested formulations were determined.

Uptake of SLNs in Pulmonary Cell Lines

To examine the effects of particle charge and surface modification with AL on the cellular uptake of SLNs, qualitative and quantitative in vitro uptake experiments were performed using fluorescently labeled SLNs (Cou-SLNs). Qualitatively, particle internalization after 6 and 24 h was monitored using CLSM 3D-time-lapse imaging of the z-stacks. Data evaluation and 3D reconstruction were performed using ZEN software (Zeiss, Germany). The quantitative uptake efficiency was determined in terms of the fluorescence intensity (I) of the lysed cells, following the protocol described by Shi et al[33] (Supplementary Materials).

Table 1 Composition* and Colloidal Properties of SLNs

SLN Code	QSI	CS	AL	Particle Size (nm)	PdI	ζ-Potential (mV)	Yield (%)
F1	-	-	-	143.4 ± 0.329	0.181 ± 0.004	−19.6 ± 0.265	75.22 ± 1.7
F1-AL	-	-	+	208.6 ± 1.082	0.199 ± 0.008	−12.1 ± 0.071	
F2	+	-	-	192.1 ± 0.21	0.211 ± 0.003	−9.48 ± 0.24	75.12 ± 3.38
F2-AL	+	-	+	212.4 ± 1.286	0.208 ± 0.093	−7.2 ± 0.85	
F3	-	+	-	200.4 ± 3.88	0.259 ± 0.021	11.7 ± 0.321	82.12 ± 1.27
F3-AL	-	+	+	206.7 ± 0.818	0.256 ±0.002	−9.4 ± 0.133	
F4	+	+	-	187.6 ± 2.45	0.229 ± 0.014	8.5 ± 0.318	68.14 ± 1.3
F4-AL	+	+	+	193.6 ± 0.39	0.212 ± 0.005	−14.8 ± 0.681	
Cou-F1	-	-	-	206.2 ± 0.4619	0.193 ± 0.005	−17.8 ± 0.721	
Cou-F1-AL	-	-	+	212.8 ± 0.601	0.264 ± 0.029	−17.9 ± 0.351	
Cou-F3	-	+	-	212 ± 1.061	0.248 ± 0.074	8.57 ± 0.415	
Cou-F3-AL	-	+	+	225.6 ± 0.581	0.251 ± 0.068	−8.71 ± 0.114	

Note: *Each formulation contained gelucire as a lipid and poloxamer 407 as a stabilizer.

Penetration of SLNs in Artificial Biofilm-Sputum Model (ABSM)

Artificial Sputum Medium (ASM) was prepared as reported by Kirchner et al[34] and supplemented with hydroxyethyl cellulose (1% w/v) to impart high viscosity[35] in addition to sodium alginate (1.5% w/v) to mimic the biofilm extracellular matrix and to investigate the effect of alginate lyase on particle penetration.

The diffusion of labeled SLNs was evaluated by the Transwell permeation study (the procedure was modified based on Friedl et al[36] and Torge et al[11]) and 3D-time laps imaging using CLSM (the technique was established in-house as previously described by Nafee et al[35]), as detailed in the Supplementary Materials.

Preparation and Characterization of Respirable SLN-Embedded Microparticles (MPs)

To prepare inhalable microparticles, cationic and anionic coumarin-labeled SLNs were spray-dried in the presence of carrier system blends of mannitol, maltodextrin, and leucine at a carrier: SLN ratio of 3:1 (w/w). The MP yield and dye content were measured as described in the Supplementary Materials. The size and morphology of MPs were investigated using SEM. To investigate the effect of spray drying on SLN stability, the size of SLNs after mixing with the carrier solution prior to spray drying and that of the recovered SLNs after MP reconstitution was measured. The aerodynamic behavior of spray-dried MPs was investigated using a next-generation impactor (NGI). The relevant in vitro aerosolization parameters were determined, including the mass median aerodynamic diameter (MMAD), emitted dose (ED), emitted dose fraction (EF), fine particle dose (FPD), and fine particle fraction (FPF), in addition to the geometric standard deviation (GSD), as detailed elsewhere.[37,38]

Antimicrobial Activity of SLNs

Antimicrobial Activity of SLNs on P. aeruginosa Strains

Four reference strains of *P. aeruginosa* were used to study the growth inhibitory effects of plain and QSI-loaded SLNs in the presence and absence of AL. These were wild-type PAO1, highly virulent strain PA14, nonmucinolytic strain RP37, and stable mucoid strain NH57388A. The organisms were grown either in Luria-Bertani (LB) medium or ASM to investigate the effects of nutrients and environmental conditions on microbial growth and biofilm formation using optical density (OD_{600}) measurements. As detailed in the Supplementary Materials, 2-fold serial dilutions of the free or nanoencapsulated QSI (corresponding to QSI concentrations of 4.7–75 μM), in addition to equivalent dilutions of plain nanocarriers, were performed to study the inhibitory effect on planktonic *P. aeruginosa*, biofilm formation, and *P. aeruginosa* established biofilms.

Antimicrobial Activity of SLNs on P. aeruginosa Clinical Isolates

P. aeruginosa clinical isolates (17 isolates) were collected from patients presenting to Alexandria Main University Hospital (Alexandria, Egypt) under the discretion of the treating physicians as part of the patients routine medical care (No decisions affecting the patients' immediate care were made based on the current study). Ethical approval was obtained from the Alexandria University Research Ethics Review Committee, Alexandria, Egypt. The isolates were screened for their potential to form biofilm via crystal violet adherence assay described in the Supplementary Materials. Biofilm forming isolates were those having OD values higher than the cut-off OD (ODc) taken as three standard deviations above the OD of the negative control. Five isolates (P10, P11, P13, P20 and P21) proved potential to form biofilm and were selected for further investigations. SLN formulations were incubated with planktonic bacteria and the corresponding biofilms to determine the percent growth inhibition and antibiofilm activity, respectively.

Assessment of P. aeruginosa Viability via Live/Dead (L/D) Assay

Biofilm viability of *P. aeruginosa* reference strains after incubation with plain and QSI-SLNs (at concentration equivalent to 9.4 μM QSI) in LB medium was investigated by CLSM following Live/Dead staining using SYTO-9 and propidium iodide (PI) to stain live and dead bacteria, respectively (Thermo Fisher Scientific, Waltham, MA, USA), Supplementary Materials.

The Effect of SLNs on Biofilm Extracellular Matrix

The impact of SLNs on the biofilm matrix was verified using calcofluor-white dye, which stains the extracellular polysaccharide matrix in blue in combination with staining of living cells with SYTO-9, as described above, followed by CLSM 3D-time-lapse imaging.

Uptake of SLNs in P. aeruginosa Biofilm

Cou-SLNs were incubated with *P. aeruginosa* biofilms grown overnight in LB medium at 37 °C for 3 h. The PI-stained biofilms were fixed for CLSM examination.

Statistical Analysis

Data are expressed as means ± standard deviation (SD). Statistical analyses were performed by *t*-test and one-way analysis of variance (ANOVA) using the SPSS software. Statistical significance was set at $p < 0.05$.

Results and Discussion

Physicochemical Characterization of SLNs

Colloidal Properties

Table 1 depicts the impact of payload (QSI/coumarin), chitosan coating, and surface functionalization with alginate lyase on the colloidal properties of SLN formulations. The gelucire-based SLNs were approximately 143 nm in diameter, with a negative surface potential (–19.6 mV). Loading SLNs with either QSI (F2 SLNs) or coumarin-6 (Cou-F1 SLNs) and surface functionalization with AL (F1-AL SLNs) enlarged the particles by 50–60 nm with corresponding reduction in ζ-potential up to –9.5 mV (F2 SLNs), Table 1.

Coating particles with CS (F3 SLNs) reverted the ζ-potential to +11.7 mV but obviously did not impact much on the size with an average size of 200 nm, Table 1. Low-molecular-weight chitosan (LMW-CS) was chosen because of its convenient particle size, efficient surface coating, and better water solubility under neutral conditions than those of high-MW CS. It, further, offered high number of free amino groups on the surface to conjugate AL.[9] The immobilization of AL is based on the electrostatic effect of overcompensating the surface charges and turning the ζ-potential again negative (–9.4 mV).

Labeled SLNs were comparatively larger (>205 nm), especially those bearing CS and AL; however, considering the size distribution, the effects were not pronounced (Table 1).

pH of SLN formulations ranged from 4.54 to 6.05 with a shift to lower pH in the CS-coated SLNs.

Insight into cystic fibrosis pathophysiology revealed that diminished functionality of the CF transmembrane conductance regulator (CFTR) reduces bicarbonate secretion into the airway lumen, resulting in a decreased pH of the airway surface liquid (ASL) to 6.81–6.89.[39] Under these CF environmental conditions, alginate lyase is catalytically active. Meanwhile, the antibacterial and cellular binding activity of chitosan are related to its state of protonation (pKa = 6.3). However, such pH perturbations may be abolished by age,[1] thus, reducing the efficiency of both AL and chitosan.

Particle Morphology

SLNs appeared spherical with a smooth surface and an average particle size distribution analogous to the size measurements by dynamic light scattering (Figure 1A). The TEM images showed no signs of particle aggregation. The QSI-loaded SLNs (F2 and F4) did not display any crystals, indicating drug encapsulation in the molecular state. It is believed that the organization of the lipid matrix, stabilizing agents, and active ingredients in SLNs, together with their relationship to one another, dictates their behavior as drug carriers.[40]

Thermal Properties of SLNs

Thermograms for F1, F2, F3, and F4 SLNs (Figure S1) showed that all excipients used were completely in crystalline form, with the two sharp peaks around 40 ± 1 and 54.5 ± 1.5°C, corresponding to the lipid and emulsifier, respectively. For a detailed description of the DSC thermograms, refer to the Supplementary Materials. Table S1 shows the melting peak (T_m) and corresponding enthalpies. The crystalline behavior of lipids and possible polymorphic changes, among other factors, strongly influence particle size, stability, and drug entrapment.[40] During heating or cooling, lipids tend to undergo structural changes according to their chemical structure. Depending on the composition and preparation process, lipids in the internal structure of the particles can have various conformations, such as liquid crystals, gels, or crystalline lamellar phases.[40] Immobilization of AL with LMW-CS was shown to remarkably improve its thermostability at 37 °C and 45 °C for 1 h, while maintaining its enzymatic activity.[9]

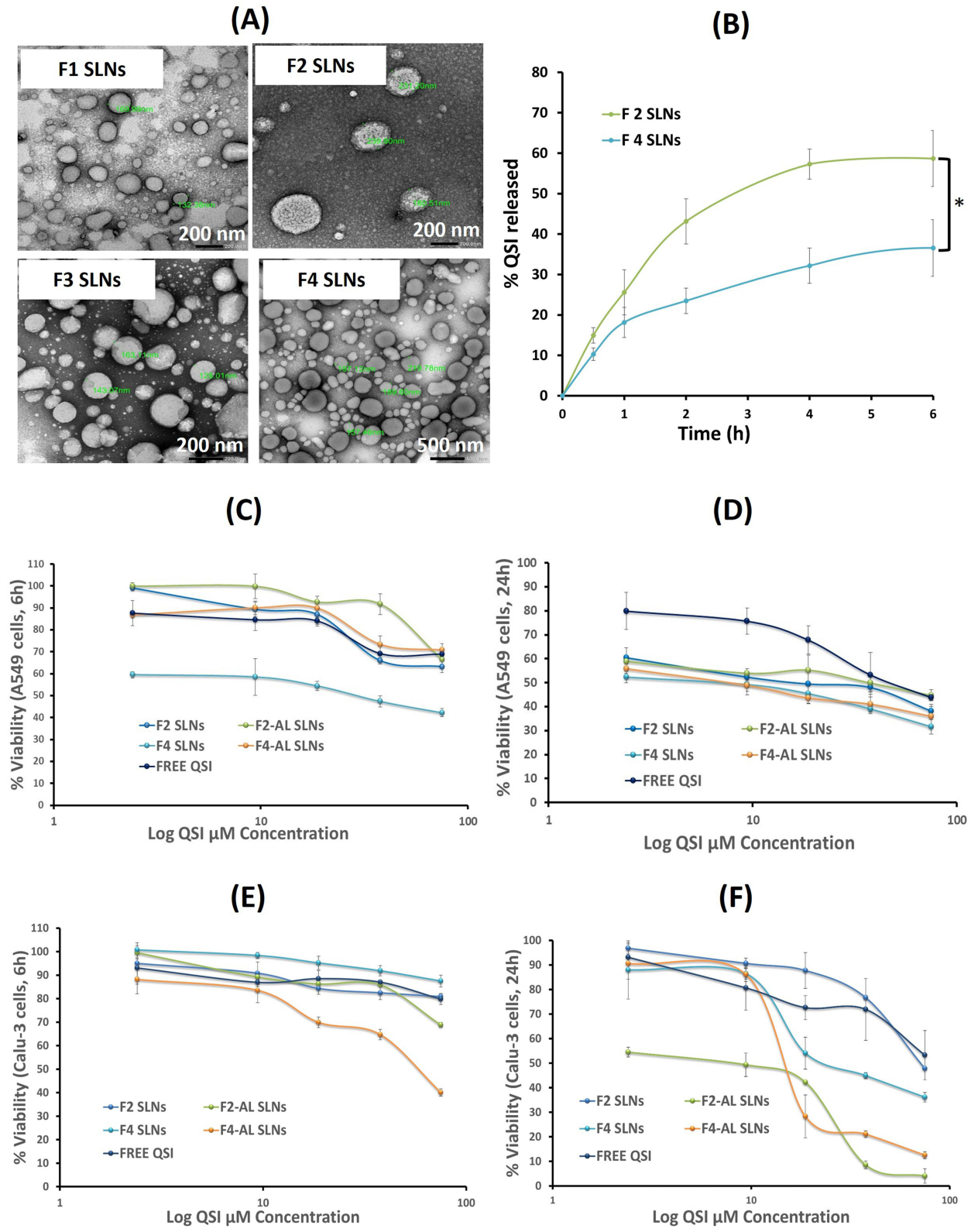

Figure 1 (**A**) TEM images F1 SLNs, F2 SLNs, F3 SLNs, and F4 SLNs; (**B**) In vitro release of QSI from F2 and F4 SLNs in SLF (*Statistically significant difference, two-way ANOVA with Tukey's post-hoc test, $p < 0.05$); (**C**) Viability of A549 cells following 6 h incubation with QSI-loaded SLNs; (**D**) Viability of A549 cells following 24 h incubation with QSI-loaded SLNs; (**E**) Viability of Calu-3 cells following 6 h incubation with QSI-loaded SLNs; (**F**) Viability of Calu-3 cells following 24 h incubation with QSI-loaded SLNs. Data represent mean values (n = 3) ± SD.

Confirmation of AL Functionalization via FTIR Spectroscopy

A comparison between the FTIR spectra of pure CS, AL, and SLNs before and after immobilization with alginate lyase was carried out to verify surface immobilization, as described in the Supplementary Materials and Figure S2.

The immobilization of alginate lyase on SLNs (F1-AL and F3-AL SLNs) resulted in strong absorption bands between 3000 and 3500 cm^{-1} indicating the presence of the enzyme, in addition to other important bands between 1541 and 1700 cm^{-1} corresponding to the N–H bending vibrations of amide II and the C–O stretching vibrations of amide I, respectively (Figure S2). FT-IR data are in line with previous reports.[9,31,41] Wan et al[31] referred to the characteristic band of amide I at 1670 cm^{-1} to confirm the presence of AL on the surface of silver nanocomposites. Covalent binding of alginate lyase on cross-linked chitosan nanoparticles was reported for AL-immobilized chitosan nanoparticles by Mohapatra.[41]

Entrapment and Loading Efficiency of QSI and in vitro Release

Data showed high EE in the range of 90–99% for both negatively and positively charged lipid formulations, with a corresponding loading of 12.48 ± 0.56 and 12.33 ± 0.23%, respectively. This reflects the suitability of the formulation technique, choice of lipid/emulsifier combination, and ratio that offers promising incorporation of payload. Noteworthy, the QSI concentration added is equivalent to 150 µM and represents the maximum loading capacity. The loaded concentration is 75-time the required effective concentration ensuring anti-virulence activity (2 µM) as per the pyocyanin assay data published earlier.[22]

A release study was carried out in SLF to mimic the microenvironment of the lungs. F2 and F4 SLNs provided a sustained release of the drug for >6 h (Figure 1B). We previously reported a more controlled release rate of QSI in SLF than in PBS; the excessive variety of components in the former might partially restrict particle swelling and limit drug dissolution and diffusion.[26]

An initial burst between 15 and 30% was recorded within the first hour, Figure 1B), which may be related to the crystallization rate of the lipid and obviously its melting point. Lipids tend to solidify faster during the cooling step, forming the inner core while expelling the drug towards the periphery, causing premature release. An effective concentration of QSI is required soon after administration to act on the bacterial biofilm. The release of QSI from F2 SLNs increased significantly with time to reach a maximum of 60% after 6 h (Figure 1B, two-way ANOVA with Tukey's post hoc test, $p < 0.05$), which is a typical behavior of gelucire-based delivery systems (eg, minitablets, granules, and beads).[42] QSI displayed comparable release rates from compritol-based SLNs, whereas tristearin-based SLNs allowed the release of no more than 10% QSI over 8 h.[26]

QSI release was significantly hampered by coating SLNs with chitosan (F4 SLNs), reaching only 38% after 6 h relative to F2 SLNs (Figure 1B, two-way ANOVA with Tukey's post-hoc test, $p < 0.05$). As a pH-responsive polymer, chitosan forms a gel network on NP surface under basic conditions (pH 7.4), hindering drug liberation. At pH values below its pKa (6.3), protonated amino groups induce solubility of the surrounding chitosan layer; a faster diffusion can thus be predicted.[43] Congruent with these findings; chitosan-coated nanoparticles elicited sustained release of numerous cargos (eg, dexamethasone, curcumin, ibuprofen) compared to naked counterparts.[43–45]

Effect of QSI-SLNs on Viability of Pulmonary Cell Lines

QSI-SLNs were designed to target bacteria within the biofilm. Thus, the detrimental effect on pulmonary cells is unintended, although it is worth investigating. The effect of drug loading, particle charge, concentration, immobilization with AL, as well as incubation time, were verified on both alveolar (A549) and bronchial (Calu-3) cell lines, Figure 1C–F. Data for unloaded formulations can be checked in the Supplementary Materials, Figure S3A–D.

Following 6 h incubation with loaded SLNs, A549 retained >80% viability in the concentration range (2.4–18.75 µM QSI) in most cases, apart from chitosan-coated SLNs (F4 SLNs) showing viability below 60%, Figure 1C). This reduced viability was not obvious for the corresponding plain particles (F3 SLNs), where above 60% viability was recorded for all SLN concentrations investigated, Figure S3A). Longer incubation period with SLNs (24 h) resulted in around 20%

reduction in viability relative to 6 h incubation with either plain or loaded counterparts, Figures 1D and S3B (statistically significant difference, Two-way ANOVA with Tukey's post hoc test, $p < 0.05$).

Surface immobilization of SLNs with AL improved A549 cell viability. Although insignificant differences were recorded for negatively charged F1 and F2 SLNs, significant impact was noted in case of CS-coated SLNs (two-way ANOVA with Tukey's post hoc test, $p < 0.05$), whereby F4-AL SLNs showed >25% higher viability compared to F4 SLNs after 6 h, Figure 1C and D). Noteworthy, effective anti-virulence activity was confirmed at QSI concentration below 2 µM, where the maximum concentration investigated in the pyocyanin assay was 15 µM.[22] This QSI concentration corresponds to SLN concentration in the range of 5.3–40 µg/mL). Reflecting this on the viability data (6 and 24 h), it can be concluded that within the effective concentration range, cell viability above 80 and 50%, respectively, can be ensured for all particle types as well as free QSI.

Determination of the cytotoxic concentration (CC_{50}) after 6h-incubation was not possible because of the high viability of all samples at all concentrations, except for F4-SLNs with a CC_{50} of 30 µM (equivalent to 80 µg/mL SLNs). One of the main advantages of SLNs is that the lipids used are generally recognized as safe (GRAS) for which metabolic pathways exist. Gelucire is the family of vehicle derived from mixtures of mono, di and triglycerides with PEG esters of fatty acids. Gelucire 43/01 is a hard fat as per European pharmacopoeia (EP) and National formulary (NF). Owing to its extreme hydrophobicity, it was extensively formulated by melt granulation or melt extrusion techniques for capsule filling and tabletting, as an effective carrier in multi-unit floating drug delivery systems, micro- and nano-emulsions. Possible cytotoxic effect was reported for gelucires with higher HLB values and more pronounced surface-active characters. Special consideration might be given to the toxic aspects of surfactants. The concentration-dependent toxicity of poloxamer 188-stabilized SLNs was reported, whereas poloxamer 407 was found to be much safer.[46] Poloxamer can interact with multidrug resistant cancer cells resulting in chemosensitisation of cancer cells. The pharmacological target(s) of this cytotoxicity remain(s) unclear. This anticancer action includes complex mechanisms involving fluidisation of the cellular membrane, ATP depletion, inhibition of drug efflux and reduction in GSH/GST detoxification activity.[47]

Table 2 depicts the CC_{50} values for the samples tested 24 h post incubation expressed as µg/mL SLNs and equivalent µM QSI. Plain AL-immobilized SLNs can be obviously tolerated at high concentration; CC_{50} value for F1-AL SLNs was above the tested range (>200 µg/mL), while that for the cationic counterpart F3-AL SLNs was 133.34 µg/mL (Table 2). Loading SLNs with QSI apparently reduced the viability of A549 cells 1–2 fold as revealed by the low CC_{50} values 17.34–100.8 µg/mL SLNs. It is still to be reminded that the recorded CC_{50} values for free and nanoencapsulated QSI are >6 µM, which is exceeding the effective concentration for anti-virulence activity.

In contrast, incubation of Calu-3 cells with SLNs for 6 h showed equally acceptable viability (>80%) in most cases, even at the maximum particle concentration tested (200 µg/mL), Figure 1E). Unlike A549 cells, F4 SLNs demonstrated the highest viability, whereas AL-CS-coated SLNs showed significantly reduced cell viability when applied at high concentrations (two-way ANOVA with Tukey's post hoc test, $p < 0.05$).

Following 24 h incubation, maximum tolerability was recorded for both plain and loaded anionic SLNs (F1 and F2 SLNs) as well as plain CS-coated SLNs (F3 SLNs) as demonstrated by their high CC_{50} values (>160 µg/mL) in Table 3. In contrast to the excellent viability of A549 cells with AL-modified SLNs, the viability of Calu-3 cells was dramatically affected after 24-exposure to either plain or QSI-loaded AL-SLNs (Figures 1F and S3D). The significant negative influence exerted by AL

Table 2 CC_{50} Values of Viability Testing on A549 Cells Following 24 h Incubation with SLNs

Plain SLNs	CC_{50} (µg/mL)	QSI-Loaded SLNs	CC_{50} (µg/mL)	CC_{50} (µM)
F1	80	**F2**	44.54	16.7
F1-AL	>200	**F2-AL**	100.8	36.5
F3	66.67	**F4**	17.34	6.5
F3-AL	133.34	**F4-AL**	21.34	8
		Free QSI	–	50

Table 3 CC_{50} Values of Viability Testing on Calu-3 Cells Following 24 h Incubation with SLNs

Plain SLNs	CC_{50} (µg/mL)	QSI-Loaded SLNs	CC_{50} (µg/mL)	CC_{50} (µM)
F1	200	**F2**	168.67	70
F1-AL	6	**F2-AL**	21.34	8
F3	164	**F4**	58.67	22
F3-AL	25	**F4-AL**	40	15
		Free QSI	–	>75

(two-way ANOVA with Tukey's post hoc test, $p < 0.05$) is then cell and concentration dependent. Si et al[48] recently combined mesoporous silica with alginate and melittin in presence of alginate lyase to control melittin release. The effect on ovarian cancer cells (SKOV3) was evaluated in terms of viability, invasion, migration assays, ROS levels, apoptosis-related proteins, and mitochondrial function tests. Cellular disruption and digestion were observed when 1 µM alginate lyase was employed. In addition, a dose-dependent decrease in the mitochondrial membrane potential was observed. It is to be noted that the concentration of AL used in the current study is far below that reported by Si et al[48]

Uptake of SLNs in Pulmonary Cell Lines

Although internalization of the formulated SLNs in the pulmonary epithelium is not the intention, studying their fate post-administration remains a concern in combination with toxicity evaluation. In parallel to the viability assays, both A549 and Calu-3 cells were designated as model alveolar and bronchial adenocarcinoma cell lines, respectively.

CLSM

As illustrated in Figure 2A, positively charged SLNs (Cou-F3 SLNs) were readily internalized in A549 cells compared to their negatively charged counterparts (Cou-F1 SLNs), which was more obvious in 24 h-treated cells. Surface modification with AL significantly improved the uptake of Cou-F1-AL SLNs compared to that of unmodified candidates (Cou-F1 SLNs), particularly after longer incubation periods. In contrast, extensive uptake of the CS-coated SLNs with and without AL (Cou-F3 SLNs and Cou-F3-AL SLNs) was observed at both time points (6 and 24 h). The potential of chitosan to empower the interactions with anionic cell membranes has been extensively reported.[44,49] Analogous uptake behavior was previously reported by Taetz et al[50] for chitosan-coated PLGA nanoparticles in A549 cells, confirming their direct dependence on the chitosan content and incubation periods. Labeled SLNs were observed as point-shaped green fluorescent areas, suggesting their entrapment in intracellular vesicles (Figure 2).

In the case of Calu-3 cells, confocal z-stacks (Figure 2B) confirmed the localization of green spots below the cell membrane in the cytoplasmic compartment, whereas no fluorescence was detected with the free dye. In comparison to A549 cells, the uptake of SLNs by Calu-3 cells was low. Their ability to build mucus at the air-liquid interface and firm tight junctions provides robustness and barriers toward particle internalization.

Despite their wide application in preclinical testing, both A549 and Calu-3 are human cancer cell lines that exhibit discrepancies in division rate and barrier properties relative to healthy primary pulmonary epithelium. Previous studies demonstrated extensive uptake of CS-coated PLGA nanoparticles in A549 cells, while they remained colocalized with the cell membrane of primary alveolar epithelial cells (hAEpC) for up to 48 h.[50] Furthermore, one can argue that particle uptake predicted upon CF epithelium topped with dense mucus encompassing mucoid bacterial biofilms would be quite diverse.

Quantitative Estimation of Uptake Efficiency

Measurement of fluorescence intensity of lysed A549 cells was carried out to get quantitative estimation of uptake efficiency. In accordance with microscopic observations, overnight exposure offered 2–3 times higher uptake efficiency than 6 h. In addition, immobilization with alginate lyase improved uptake by ≥1.5 times, Figure 3A (statistically significant difference, paired *t*-test, $p < 0.05$). Despite the negative surface charge, the increased uptake of

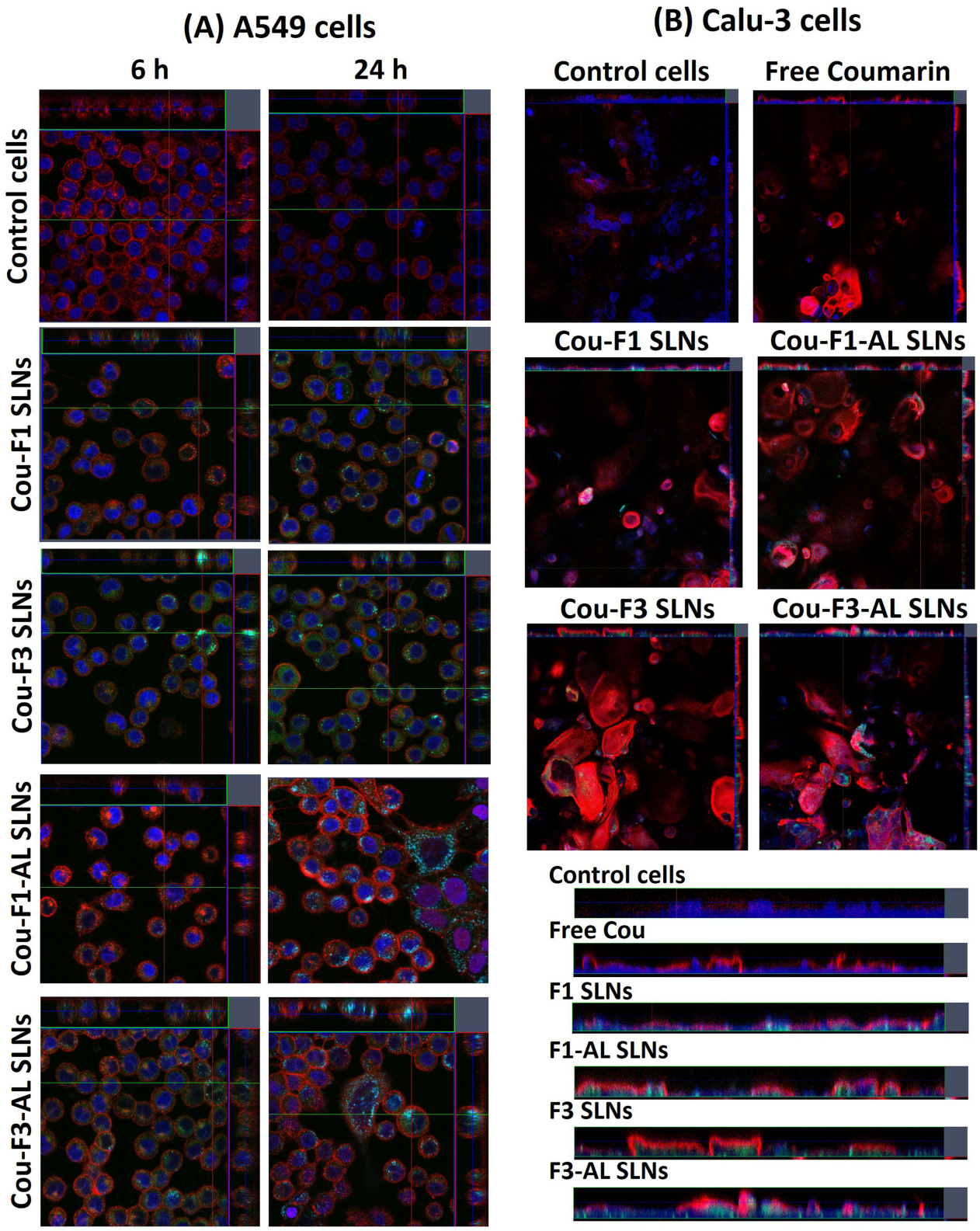

Figure 2 Confocal images illustrating the uptake of coumarin-labeled SLNs in: (**A**) A549 cells following 6 and 24 h incubation, and (**B**) Calu-3 cells after 24 h incubation (bars at the bottom right represent z-stacks).

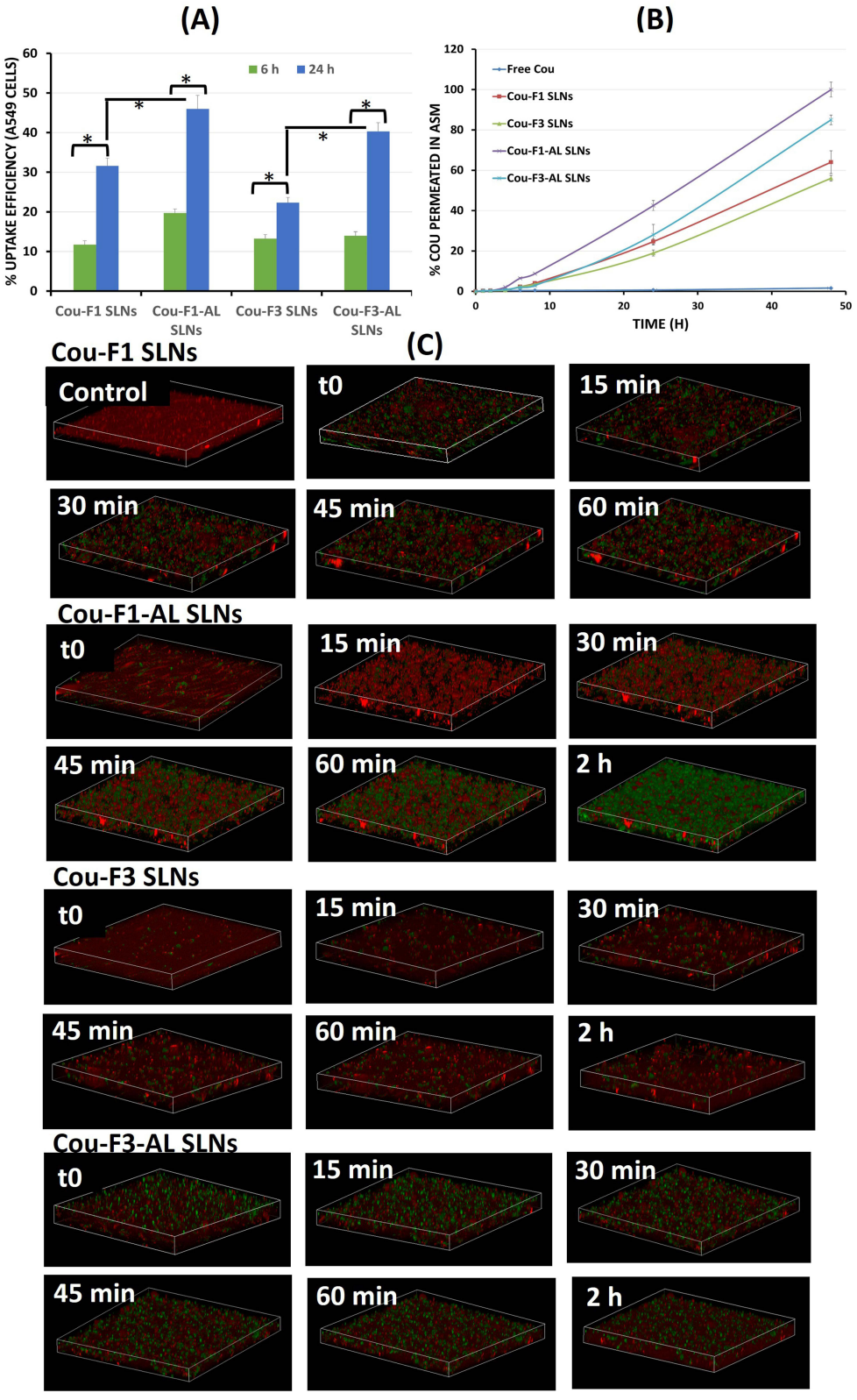

Figure 3 (**A**) Quantitative estimation of uptake efficiency of coumarin-labeled SLNs in A549 cells via Transwell technique following 6 and 24 h incubation (*Statistically significant difference, paired *t*-test, p <0.05); (**B**) Permeation efficiency of coumarin-labeled SLNs in artificial biofilm sputum medium; (**C**) 3D-time lapse confocal stacks showing diffusion of different coumarin-labeled SLNs in artificial biofilm sputum medium over 1–2 h.

AL-immobilized particles suggests uptake mechanisms other than classical ionic interactions with the cell membrane. However, the molecular interactions between AL and human lung epithelium remain unknown. In line with this finding, it was reported that the addition of alginate lyase to melittin-loaded nanoparticles (without surface immobilization) showed concentration-dependent improvement in the cellular uptake studied on ovarian cancer cells.[48]

Penetration of SLNs Across Artificial Biofilm Sputum Medium

To reach lung-residing bacteria and achieve effective eradication by therapeutic agents, biological barriers such as the extracellular sputum matrix and biofilm need to be overcome.[3] The ability of formulated SLNs to penetrate CF sputum dictates their effectiveness against *P. aeruginosa* in CF lungs. The penetration of coumarin-labeled positively and negatively charged SLNs with and without surface immobilization with alginate lyase was verified on ASM supplemented with alginate as the main component of the extracellular matrix and HEC as a viscosity-imparting agent.[51]

Efforts to mimic the in vivo nutritional environment of lungs yielded a variety of in vitro culture compositions referred to as "artificial sputum media". The ASM model has been recently used to investigate bacterial physiology, biofilm morphology, and antibiotic susceptibility in addition to studying the adaptation of pathogens to the CF lung and testing the effectiveness of antibacterial therapeutics.[52] Although ASM can be considered more biorelevant than conventional mucin solutions, the absence of bacterial colonies and matrix components would shade probable imperative interactions of nanotherapeutic entities and biofilm. In a previous study, we appraised the application of ASM, real CF sputum and air-interface Calu-3 cells as a platform for penetration experiments.[35] In the current study, investigating the effect of enzyme-linked SLNs urged the presence of the substrate (alginate) as supplement in ASM.

Transwell Permeation Study

SLN permeation through the artificial biofilm-sputum model was generally a slow process, remaining below 10% during the first 8 h. As illustrated in Figure 3B, labeled SLNs decorated with alginate lyase (Cou-F1-AL and Cou-F3-AL SLNs) showed faster migration than undecorated SLNs, whereby the fluorescence intensity almost doubled in the presence of AL at all time points (statistically significant, two-way ANOVA with Tukey's post hoc test, $p < 0.05$).

Interestingly, significantly higher fluorescence intensity was observed for negatively charged SLNs (Cou-F1 and Cou-F1-AL SLNs) than for the CS-coated candidates (Cou-F3 and Cou-F3-AL SLNs), Figure 3B, (two-way ANOVA with Tukey's post hoc test, $p < 0.05$). Meanwhile, free coumarin-6 displayed negligible fluorescence, presumably because of the quenched fluorescence of the hydrophobic probe in the aqueous milieu.[53]

Nanocarriers penetrate the biofilm matrix. The potential for biofilm diffusion is a function of their size, charge, and surface chemistry. Nevertheless, both positively and negatively charged NPs display reduced diffusion velocities and binding to bacterial biofilms via diverse mechanisms. While anionic polystyrene NPs can bind to the proximity of bacterial cells via hydrophobic interactions, their cationic counterparts might attach to wire-like components, presumably biofilm polymers, and/or negatively charged DNA.[15]

Relevant to this discussion, the emulsifier layer on nanoparticle surface plays a crucial role in biofilm penetration process. We previously demonstrated that SLNs stabilized with poloxamer 407 exerted higher diffusion in both ASM and CF sputum compared to Tween 80- and PVA-stabilized SLNs.[35] In accordance with that, coating polystyrene NPs with PEG was described to exhibit a 90-fold higher diffusion rate in 10 μm-thick mucus versus noncoated NPs.[54] Poloxamer 407 – the triblock copolymer (PEO-PPO-PEO) comprising polyethylene oxide (PEO) and polypropylene oxide (PPO) – covers F1-NP surface with a dense hydrophilic brush of PEO that incites excellent penetrability.[35] Coating SLNs with the mucoadhesive polymer chitosan was certainly allied to a different performance. Owing to the advantages of mucoadhesion and prolonged residence time, weak penetrability remains a major concern.

3D Time-Lapse Confocal Imaging

3D time-lapse confocal imaging represents a promising approach to visually investigate nanoparticulate diffusion in biofilms, as reviewed by Schlafer and Meyer.[55] Alexa Fluor-WGA is a well-reported fluorescently labeled lectin with selective-binding characteristics to the carbohydrate-containing extracellular matrix of *P. aeruginosa* biofilms.[56]

The z-stacks (Figure 3C) showed gradual time-dependent particle diffusion at varying rates and extent over 2 h. The maximum green fluorescence was observed for Cou-F1-AL, followed by Cou-F1 > Cou-F3-AL > Cou-F3 SLNs. Confocal stacks were in line with the Transwell diffusion experiment, confirming the potential of alginate lyase to break down the alginate mesh (the primary component in bacterial biofilms), resulting in reduced viscosity and weakened biofilms with faster and deeper particle penetration. According to Messiaen et al,[57] the presence of DNase I also improved the diffusion of charged polymeric NPs 10 times in the biofilm.

In contrast, the chitosan-coated SLNs exhibited minimal penetrability. Indeed, there are multiple lines of evidence that support a predilection toward this behavior; electrostatic interactions between cationic chitosan and anionic alginate/DNA in biofilms and/or sialic acid residues in mucin would presumably capture the particles on the top and hinder their diffusion. Nonetheless, several studies have reported the potential of chitosan-coated PLGA NPs to penetrate artificial mucus.[54,58] Penetration of labeled chitosan nanoparticles in *Staphylococcus aureus* and *P. aeruginosa* biofilms was improved when functionalized with DNase.[59,60] Analogous behavior was observed with AL-functionalized SLNs. The reported approaches for AL-immobilized chitosan NPs lack data on sputum and/or biofilm penetration.[8,9]

Characterization of Respirable SLN-Embedded Microparticles (MPs)

To ensure sufficient deposition and avoid premature exhalation of the inhaled powder nanocarriers owing to their small size, SLNs were assembled into respirable microparticles via spray drying. Cou-F1 and Cou-F3 SLNs were sprayed with a carbohydrate carrier mixture (mannitol, leucine, and maltodextrin). The carrier ratio was previously optimized elsewhere.[61] MPs were characterized in terms of yield, dye content, particle morphology, and aerodynamic behavior.

Cou-F1 and Cou-F3 MPs ensured a powder yield of 71.6 and 76.3%, respectively, with a percentage dye recovery of 98.14 and 97.84%, respectively.

SEM micrographs (Figure 4A) illustrate the morphology of the spray-dried microparticles as spherical corrugated microspheres with an average geometric diameter of 3 µm. Surface wrinkles are usually defined by collapse owing to the low glass transition temperature of mannitol counterbalanced by maltodextrin.[61]

The stability of SLNs after spray drying was verified. As depicted from Figure 4B, SLNs mixed with the carrier solution were around 20 nm larger than the original SLNs, presumably attributed to leucine, mannitol and maltodextrin coating particle surface or dispersed in solution. Further slight increase in size and PdI was reported for SLNs recovered following reconstitution of microparticles. Of interest, this increase in size and PdI cannot reflect particle agglomeration and/or aggregation.

Investigating the in vitro deposition pattern of MPs using NGI revealed comparable behavior for both formulations (statistically insignificant difference, paired *t*-test, $p < 0.05$); maximum deposition (44–60%) in stages 3–5 (equivalent to 0.94–2.82 µm cutoff diameter), Figure 4C). Relevant aerodynamic diameters are summarized in Table 4, which depicts an MMAD of 3.54 and 2.48 µm for Cou-F1 and Cou-F3 MPs, respectively.

Both particles ensured a very promising emitted dose fraction above 92% (statistically insignificant difference, one-way ANOVA, $p < 0.05$). Cou-F3-SLNs-MPs showed higher FPF of 64.52 compared to Cou-F1-SLNs-MPs (47.88) indicating major deposition in the deep lung.

Anti-Pseudomonal Activity of SLNs

The impact of the formulated SLNs on the growth of mucoid and non-mucoid strains of *P. aeruginosa* (PA01, PA14, RP37, and NH57388A) and biofilm-forming clinical isolates was explored. Predetermined concentrations of QSI-loaded negatively charged particles (F2 SLNs) were compared to those of their positively charged counterparts (F4 SLNs). In addition, the influence of AL coating (F2-AL and F4-AL SLNs) was investigated. For comparison, free QSI and plain SLNs (F1, F1-AL, F3, and F3-AL SLNs) were studied at concentrations equivalent to those of the corresponding loaded formulations. In addition to the different formulations, the effects of the culture medium (LB and ASM) on *P. aeruginosa* strains in presence of the formulations were investigated. The studied endpoints included growth inhibition of planktonic bacteria, effects on biofilm formation, and eradication of established biofilms.

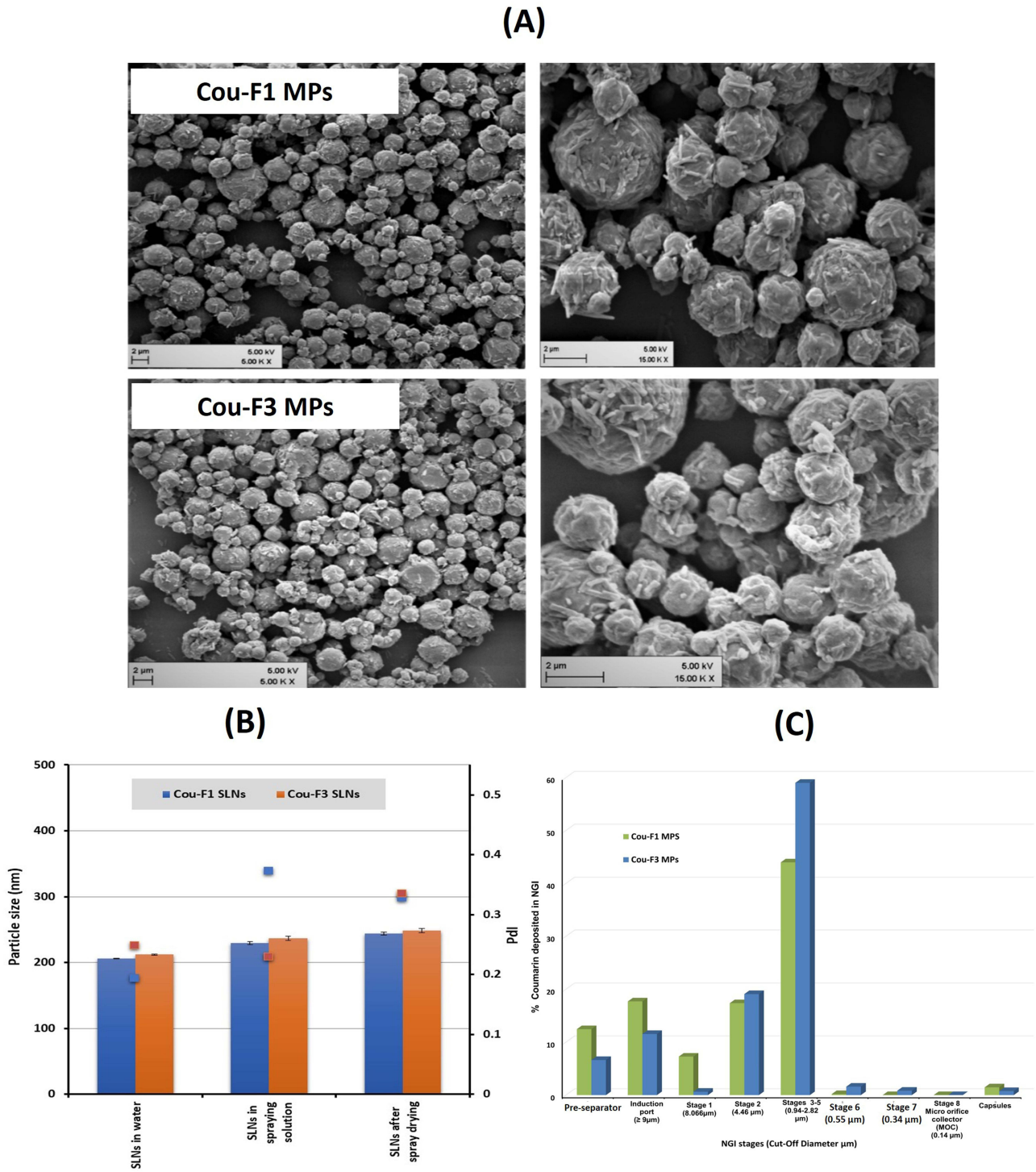

Figure 4 (**A**) SEM micrographs of SLN-embedded microparticles (scale bar 2 µm); (**B**) Colloidal stability of SLNs in the spray drying solution and after spray drying; (**C**) Deposition pattern of cou-F1 MPs and cou-F3 MPs on stages of next generation impactor.

Antimicrobial Activity of SLNs on P. aeruginosa Reference Strains

The growth inhibition graphs (Figures 5 and S4) revealed strong dependence on the *P. aeruginosa* strain, planktonic versus biofilm cells, growth medium, type of SLNs, and AL coating, as detailed below. A concentration range of 4.7–75 µM free and nanoencapsulated QSI was tested. Figure 5 shows the antimicrobial activity of SLN formulations equivalent to 18.75 µM QSI. The rest of the data are shown in the Supplementary Materials (Figure S4).

Table 4 Aerosolization Parameters of SLN-Embedded Microparticles as Determined by NGI

Aerosolization Parameters	F1-SLNs-MPs	F3-SLNs-MPs
MMAD (μm)	3.54	2.47
GSD	1.95	2.35
FPF (%)	47.88	64.52
EF (%)	92.87	97.42
% yield	71.60	76.50

Effect of SLNs on Growth of P. aeruginosa Planktonic Cells

In LB medium (Figure 5A), both PA14 and NH57388A were more sensitive than PAO1 to SLN treatment ensuring 70–95% growth inhibition when treated with AL-immobilized SLNs (F2-AL SLNs). In comparison, incubation of RP73 with F4-AL SLNs (equivalent to 18.75 μM QSI) repressed bacterial growth by 75%. Of interest, no growth inhibition of PA01 planktonic cells at QSI concentrations of up to 18.75 μM was recorded in LB medium regardless of the particle type (Figure 5A). These data are coherent with the goal of the study. Indeed, bacterial killing that ends up with robust antibiotic resistance is not the target. One advantage to quorum quenching therapeutic approach is that it inhibits QS without killing the bacteria, which does not pressure the bacteria to develop resistance against the inhibitors, thus permitting the host immune system to clear the infection.[62]

At the QSI concentration previously reported for promising anti-virulence potential (up to 15 μM), no growth inhibition was achieved. The dependence of anti-infective effect on bacterial strain, growth medium, and incubation period, among others, is extensively reported.[62,63]

PAO1, isolated from a wound >50 years ago, is a moderately virulent strain. The broad use of PAO1 created opportunities for mutational events to yield numerous PAO1 sub-lines with various phenotypic and genetic differences.[64] In comparison, the clinical strain PA14 is highly virulent and represents the most common clonal group worldwide.[65] Although PA14 is the more virulent strain, it displays a high level of genomic conservation with that of PAO1. On the genomic level, PA14 possesses two pathogenicity islands, which carry virulence-associated genes that are not present in the genome of PAO1.[65]

Another aspect is the key difference between PA14 and PAO1 quorum sensing (QS) mechanisms. The less virulent PAO1 strain produces high levels of QslA protein, a QS deactivator, which was minimally expressed in the hypervirulent PA14 strain.[66] In addition, some strain genetic and phenotypic inconsistencies have been observed including *MexT*, a significant QS factor and fitness regulator, and *LasR* found in PAO1 strains from different laboratories. Their reported mutations affected QS signal, virulence factor, biofilm formation, and motility expression.[67]

Indeed, there is evidence that the growth behavior of *P. aeruginosa* is influenced by the growth medium. While the nutrient-rich, standard laboratory medium (LB medium) comprises tryptone, yeast extract, and sodium chloride in water,[68] ASM includes different components that mimic the lung environment, namely mucin, DNA, amino acids, and lipid source.[69] Growing *P. aeruginosa* strains in ASM instead of LB medium significantly increased their susceptibility to SLNs, where almost full growth inhibition was observed in all strains, especially NH57388A mucoid planktonic cells. Interestingly, 75–95% growth inhibition of PA14 was achieved regardless of the formulation type (Figure 5B).

It is to be carefully considered that numerous ASM recipes were reported in the literature with varying types, sources and concentrations of nutrients and were found to yield different phenotypes and chemotypes of *P. aeruginosa*, in other words, affecting microbial growth, metabolism and virulence.[70] In this study, for instance, porcine gastric mucin, the main component of most ASM, represents an unexpected source of iron, which alters the production of specialized metabolites referred to as siderophores, mainly acting as metal scavenging virulence factors in *P. aeruginosa*.[70] Siderophore production is primarily triggered by diminished levels of environmental iron. ASM with limited or no amino acid content restricts the ability of *P. aeruginosa* to produce the redox active virulence factors (phenazines).[70] Conversely, ASM supplemented with N-acetyl glucosamine induces significant production of the virulence factor pyocyanin as N-acetyl glucosamine promotes a mechanism to sense and respond to peptidoglycan.[69] Noteworthy, ASM recipe used in our experiments comprised porcine mucin, yet no N-acetyl glucosamine was added.

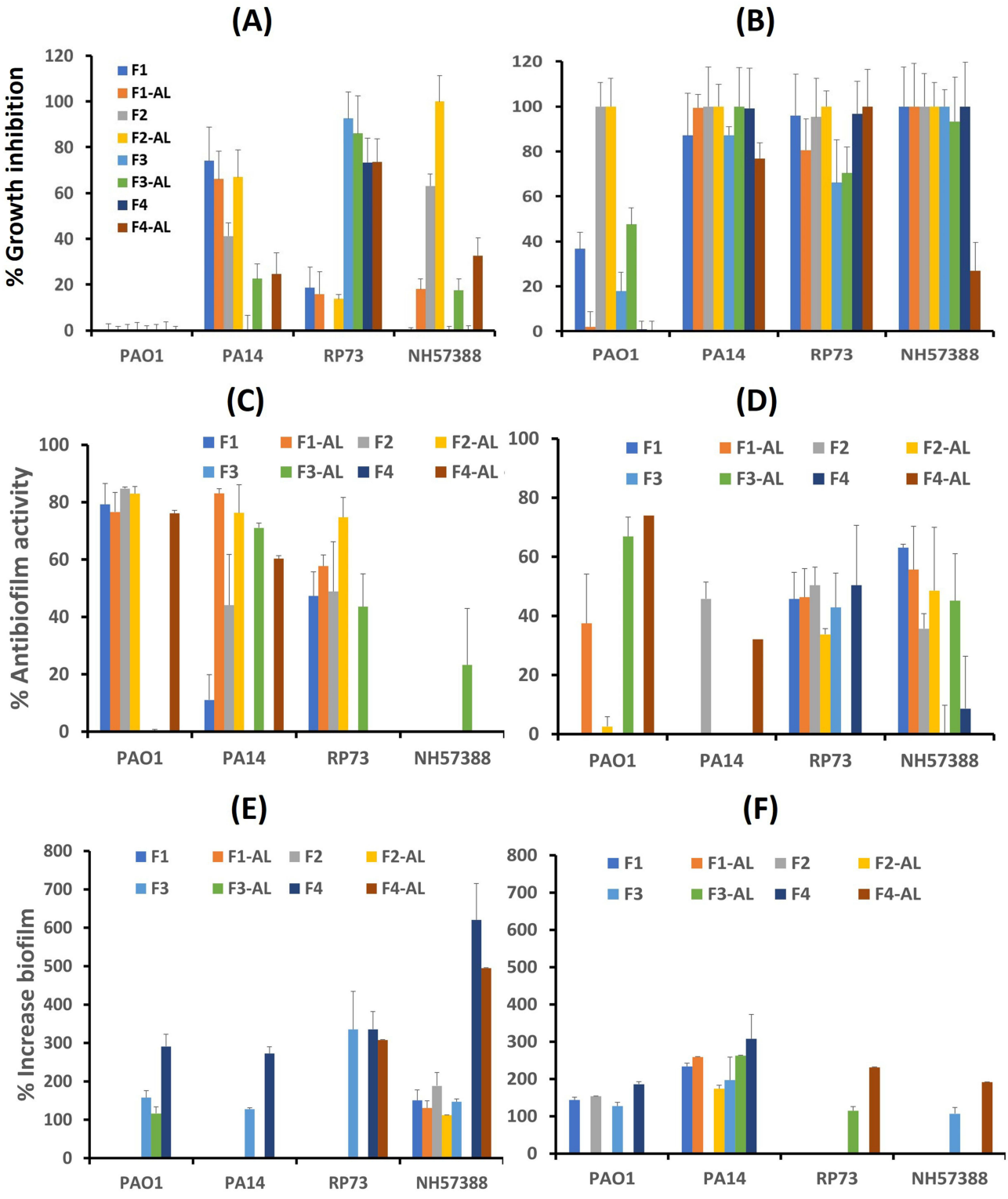

Figure 5 Antimicrobial activity of SLNs (equivalent to 18.75 μM QSI) on *P. aeruginosa* reference strains (**A**) *P. aeruginosa* planktonic reference strains in LB medium; (**B**) *P. aeruginosa* planktonic reference strains in ASM; (**C**) Antibiofilm activity in LB medium; (**D**) Antibiofilm activity in ASM; (**E**) Increase in biofilm formation in LB medium; (**F**) Increase in biofilm formation in ASM.

The antipseudomonal activity exerted by plain particles was analogous to that of their loaded counterparts (Figure S4). Wherever loaded particles showed pronounced growth inhibition, plain SLNs seemed to contribute to this effect. This could be directly related to our previous finding that plain SLNs have non-negligible anti-virulence potential, which is directly related to the anti-virulence power of the emulsifiers used.[26]

Effect of SLNs on P. aeruginosa Biofilm Formation

The developed formulations were primarily designed to target the biofilm matrix. In general, the inhibition of biofilm formation by the tested samples in LB medium was more pronounced for the PA01 > PA14 > RP73 > NH57388A strains (Figure 5C and Supplementary Materials, Figure S5). Interestingly, all SLN formulations showed distinct antibiofilm activity on PA01 biofilm in LB medium, without any growth inhibition potential of planktonically grown PA01 cells. AL-decorated negatively charged SLNs significantly hindered biofilm formation with PA14 strain by >80% over the investigated concentration range (two-way ANOVA with Tukey's post hoc test, $p < 0.05$).

PAO1 and PA14 showed discrepancies in their attachment and biofilm formation strategies. While PAO1 can quickly attach to surfaces and irreversibly progress to biofilm formation, PA14 displayed less commitment to surface attachment. This was mechanistically related to the Wsp pathway that mediates PAO1's surface recognition resulting in higher production of exopolysaccharides that promote attachment of nearby bacterial cells. PA14's surface recognition strategy, however, is driven by the Chp pathway, which adjusts cAMP concentrations to promote planktonic cell surface memory.[71] Mikkelsen et al[65] proved that PA14 has an acquired mutation in the *ladS* gene, causing a deleterious impact on the biofilm, resulting in elevated T3SS activity and increased cytotoxicity towards mammalian cells. Notably, the RetS/LadS/GacS signaling cascade is associated with virulence, in which the LadS sensor promotes biofilm formation and represses T3SS.[65]

However, the weakest antibiofilm effect of SLNs was observed in the case of mucoid NH57388A strain in LB medium, although 60–70% inhibition of biofilm formation could be registered in ASM (Figures 5D and S5A). The functionality of bacterial biofilms is associated with their microscale structures. Components of the extracellular matrix delineate the viscoelastic properties of the biofilms. Prevalence of water and soluble polysaccharides provides stress relaxation time of (0.01–3 s), while insoluble polysaccharides provide higher values of (3–70 s), and eDNA from (10–25 s) for the relevant concentrations.[72] The characteristics and matrix composition were directly tied to the growth medium. For instance, *P. aeruginosa* (ATCC 39324) biofilms grown in ASM elicited high eDNA and polysaccharide content relative to those formed in LB medium.[72] Accordingly, unbound water represents the fastest relaxation component in LB-grown biofilms, whereas slower stress relaxation components due to water with dissolved polysaccharides, insoluble polysaccharides, and eDNA were most important in the relaxation of ASM-grown biofilms.[72] The latter, thus, provided the most protective matrix that maximally hampered penetration and bacterial killing. The difference in biofilm matrix composition, as affected by the growth medium, might explain the difference in the response to SLNs between LB and ASM. Interestingly, Reighard et al[73] synthesized chitosan oligosaccharide scaffolds capable of altering the viscoelasticity of *P. aeruginosa* biofilm and transforming it into nearly elastic solids without viscous components.

Consistent antibiofilm potential was identified in plain AL-modified SLNs, as well as in free QSI and free AL, especially in the RP73 strain (Supplementary Materials, Figure S5A). AL alone displayed stronger antibiofilm power against mucoid than nonmucoid *P. aeruginosa* strains under investigation, as observed with the NH57388A strain in LB medium (statistically significant difference, two-way ANOVA with Tukey's post hoc test, $p < 0.05$). Interaction of AL with alginate within alginate-synthesizing bacterial biofilms is worth deeper insight; AL actually plays vital roles in both biosynthesis and biodegradation of alginate.[74] During alginate biosynthesis, AL contributes to the control of alginate polymer length and optimization of polymerization reaction.[75] Meanwhile, it enhances biofilm degradation to facilitate bacterial propagation in the host mucosa.[75,76] A systematic approach conducted by Lamppa and Griswold[77] revealed that enzyme-mediated biofilm disruption and antibiotic synergy are decoupled from catalytic activity. Instead, the antibiofilm effects of AL may be related to enzyme-mediated changes in the cell physiology.

Unforeseen behavior was associated with CS-coated SLNs, which displayed weak or no antibiofilm activity on *P. aeruginosa* independent of the growth medium. In contrast, a distinct increase in OD was observed, indicating promotion of biofilm formation rather than inhibition. This dictated the determination of increased biofilm formation by SLN-treated *P. aeruginosa* strains whenever applicable to study this effect. Biofilm promotion was distinguished in the case of the NH57388A strain in LB medium, as well as PA14 in ASM (Figure 5E and F). As depicted in Figure S5B, cationic SLNs (F4 SLNs) significantly induced biofilm formation (150%), even at low concentration (4.7 μM QSI), reaching up to 1000% at 75 μM in NH57388A strain (two-way

ANOVA with Tukey's post hoc test, $p < 0.05$). Neutral liposomes were favored over charged liposomes by striking a balance between mucus interaction and affinity toward bacterial cells,[78] whereas other studies have reported superior antipseudomonal activity of cationic liposomes over anionic ones.[79,80] These sometimes conflicting findings point toward an overall, incomplete understanding of the underlying mechanism.

Antimicrobial Activity of SLNs on P. aeruginosa Isolates

Of the 17 collected isolates, five *P. aeruginosa* isolates (P10, P11, P13, P20, and P21) were confirmed to have the ability to form biofilms and hence were selected for growth inhibition experiments. The effects of free QSI, plain SLNs, and QSI-loaded SLNs were studied first on the growth of planktonic *P. aeruginosa* cells, their ability to form biofilms, and already established biofilms. Growth graphs for formulations equivalent to 18.75 µM QSI are shown in Figure 6, while results for the whole concentration range tested (2–200 µg/mL formulation equivalent to 2.4–75 µM QSI) are detailed in the Supplementary Materials (Figure S6).

Effect of SLNs on Growth of Planktonic P. aeruginosa Isolates

As shown in Figure 6A, free QSI had obviously no or minor (<10%) inhibitory effects on the growth of all isolates over the concentration range studied. This is in accordance with previous data from our collaborators, who confirmed that QSI selectively targets QS-controlled virulence without affecting the growth kinetics of *P. aeruginosa* when tested on PA14 strain up to 15 µM.[22]

Of interest, all nanocarriers (F1–F4) mostly showed significant concentration-dependent growth inhibition on all strains not exceeding 65–70% at 18.75 µM QSI concentration (Figure 6A), reaching up optimal inhibition at concentrations (37.5–75 µM), Figure S6A, two-way ANOVA with Tukey's post hoc test, $p < 0.05$. The dominant effect was related to the positively charged SLNs (F3 SLNs), ensuring at least 25–100% growth inhibition in all isolates at concentrations (9.5–75 µM). In comparison, negatively charged SLNs could achieve up to 80% growth inhibition (Figure 6A and Supplementary Figure S6A). The outer membrane of *P. aeruginosa* is decorated with lipopolysaccharide (LPS). Cationic chitosan has been reported to interact with the negatively charged phosphate, pyrophosphate, and carboxylic groups of LPS.[81] This interaction significantly modulates the biological activity of LPS.[82]

Effect of SLNs on P. aeruginosa Biofilm Formation

Following the invasion of *P. aeruginosa* in CF lungs, penetration of the mucus surface and colonization are associated with a dramatic genetic transformation of the nonmucoid to mucoid (alginate-producing) phenotype. Although the nonmucoid phenotype is more virulent, the mucoid phenotype enhances pseudomonal adhesion and resistance to phagocytosis.[13] Indeed, many of the drastic, detrimental clinical manifestations of the mucoid phenotype are attributed to the phenotypic conversion conferred by alginate overproduction.[1]

Compared to planktonically grown *P. aeruginosa* isolates, SLNs elicited considerable concentration-dependent inhibitory effects on biofilm formation (Figure S6B; statistically insignificant difference, two-way ANOVA, $p < 0.05$). At the selected concentration (18.75 µM), biofilm inhibition reached 40–50% in P10 and P13 isolates, which was lower than 40% in the rest of isolates (Figure 6B). Reasonable control of QSI on biofilms was observed for the P11 and P13 *P. aeruginosa* isolates. This is in accordance with the hypothesis that QSI is mainly considered a pathoblocker disrupting bacterial virulence via by interfering with the quorum sensing cell-to-cell communication system that co-regulates biofilm formation.[18]

Despite the clear fluctuation in antibiofilm potential from one isolate to another, the non-negligible impact of plain SLNs on biofilm formation should be considered (Figure 6B).

Combining this with the previously reported anti-virulence activity urges the appraisal of the antipseudomonal potential of SLN components. Poloxamer 407 gel proved to be more suited to Mueller–Hinton agar during susceptibility antimicrobial testing and showed resistant phenotypes, whereby more than 60% of the strains displayed increased resistance to beta-lactams when cultured on poloxamer gel relative to Mueller–Hinton agar. The same study also showed that biofilm formation related to growth on poloxamer 407 gel.[83] Thermo-reversible poloxamer 407 hydrogels coupled

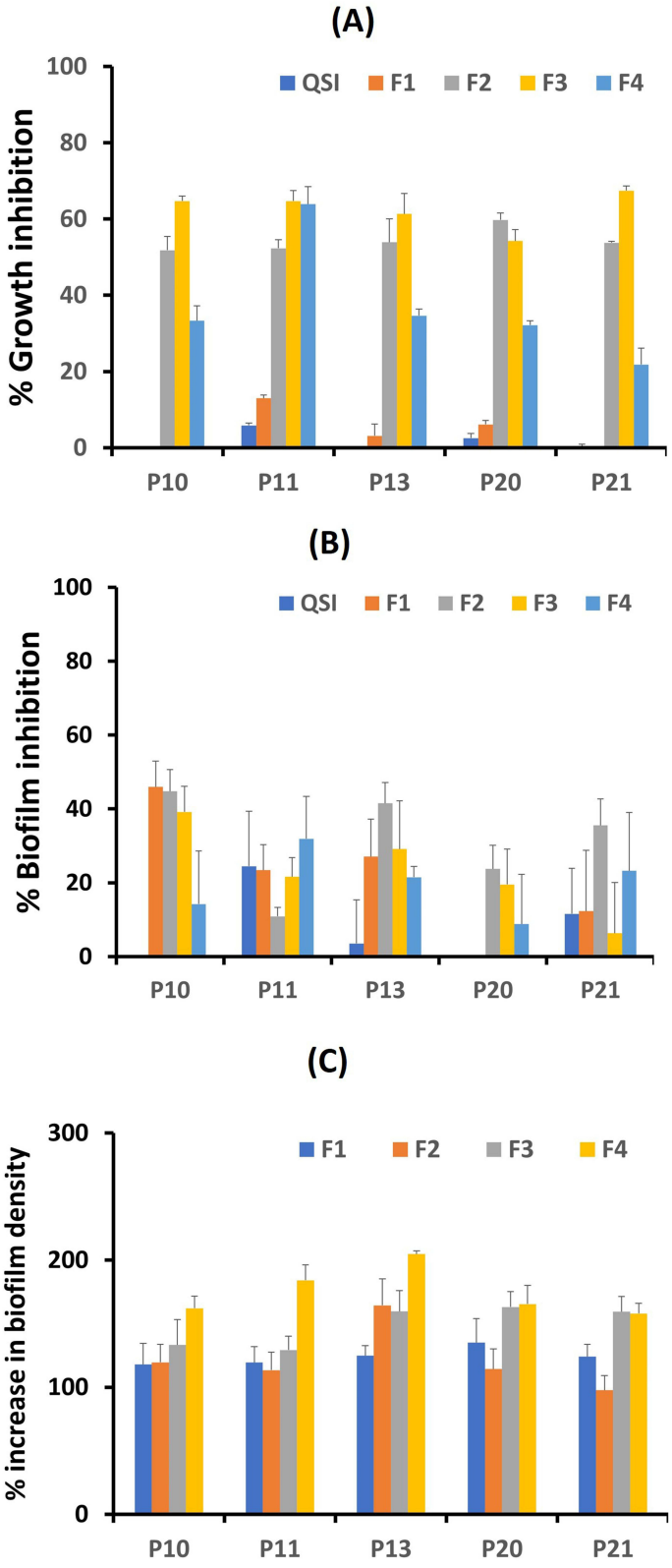

Figure 6 Antimicrobial activity of SLNs (equivalent to 18.75 μM QSI) on *P. aeruginosa* isolates (**A**) Growth inhibition of *P. aeruginosa* planktonic isolates; (**B**) Inhibition of biofilm formation of *P. aeruginosa* isolates; (**C**) Increase in biofilm formation of *P. aeruginosa* isolates.

with Live/Dead bacterial staining were elsewhere applied for antibiofilm testing.[84] Such an effect could not be observed in our study, presumably being overcompensated by other SLN components.

Considering Gelucire lipid, nanostructured lipid carriers composed of Gelucire 50/13 and oleic acid loaded with α-terpineol demonstrated notable inhibitory effect on quorum-sensing mediated virulence and biofilm formation together with more than 50% reduction of MIC compared to the free form.[85] Levofloxacin-loaded PLGA nanoparticles coated with phosphatidylcholine lipid exhibited higher antibacterial efficacy against *P. aeruginosa* biofilms rather than planktonic cells; authors suggested that the lipid coat presumably lead to variations in antibiotic activity, release rate, and biofilm cell detachment.[86] Another intriguing investigation by Alipour et al[13] reported the inability of liposomal formulations to improve the antimicrobial activity (in particular biofilm eradication) of aminoglycosides in presence of alginate in *P. aeruginosa* biofilms. According to the authors, this was attributed to certain interactions of liposomal lipids with alginate in the biofilm that presumably prohibited their interaction with the bacterial membrane.[13] This assumption was based on other studies describing alginate/lipid interaction and alginate insertion within the cationic phospholipid bilayer that might cause liposomal destabilization.[13] These findings can be extended to explain the current increase in biofilm formation observed, particularly with positively charged SLNs (Figure 6C).

Eradication of Established P. aeruginosa Biofilms

Biofilm eradication, which is as important as the inhibition or avoidance of biofilm formation, can be considered a non-negotiable rescue, especially when translated into CF infection.

Two-day-old biofilms of *P. aeruginosa* isolates were incubated with different SLNs (Figure 6C). Despite their ability to limit biofilm formation, SLNs have unexpected effects on mature biofilms. Independent of the isolate, negatively charged SLNs (QSI concentration < 10 μM) exhibited weak antibiofilm efficacy (<20%). Above this concentration, SLNs surprisingly promoted biofilm formation, which is in agreement with the aforementioned data on *P. aeruginosa* reference strains. Accordingly, the data are presented in Figure 6C, as the biofilm density increased relative to that of the control. Following incubation of mature biofilms with SLNs, an average of 1.5-fold denser biofilm could be evidenced, exceeding 200–250% in P13 isolate (Figure S6C). Chitosan-coated SLNs showed a significantly higher tendency to promote biofilm formation (Figure 6C; two-way ANOVA with Tukey's post hoc test, $p < 0.05$). Many studies have elucidated the antimicrobial activity of chitosan,[59,87] however, these data cannot be extended to the eradication of mature biofilms. Reighard et al[73] studied the antibiofilm activity of chitosan oligosaccharide scaffolds. Even at the highest concentration tested (16 mg/mL), complete eradication of *P. aeruginosa* biofilms could not be achieved unless nitric oxide was added. Hence, it was assumed that cationic chitosan modifies the electrostatics of the predominantly anionic *P. aeruginosa* biofilm. This would then potentially enhance matrix cross-linking and contribute to biofilm cohesion.[73] In line with that, Germoni et al[88] reported considerable increase in biofilm mass following treatment with low concentration of gentamicin, presumably related to stimulation of biofilm matrix production by subinhibitory concentrations of the aminoglycoside antibiotic. Other conflicting findings confirmed the significant inhibition of biofilm formation by chitosan nanoparticles (75–89%) as well as *P. aeruginosa* biofilm eradication capacity; the latter was yet based on visual observation and not quantified by the crystal violet biofilm method.[89]

The discrepancy in outcomes can be related to the heterogeneity in biofilm phenotypes, divergence among isolates, and different techniques for biofilm preparation, treatment, and assessment during experimentation. Although standard laboratory models rely on bacterial biofilm formation on material surfaces, *P. aeruginosa* biofilms within the CF lung tend to be nonadherent spherical microcolonies embedded in stagnant respiratory mucin.[52] In addition, in vivo biofilms were reported to be more complex compared to those grown in laboratory media. Biofilms isolated from CF patients showed a "sponge-like" appearance with mucus or lung fluid punctuating bacterial masses, whereas in vitro biofilms were more homogenous with dense or mushroom-like structures.[90]

Effect of SLNs on Bacterial Cell Viability via Live/Dead Staining

The Live/Dead stain package relies on two nucleic acid-binding stains, SYTO-9 and PI, which differ in their spectral characteristics and ability to penetrate vital bacterial cells. SYTO-9 stains all cells green (vital and nonvital), whereas PI only penetrates cells with compromised or damaged membranes and stains them red.[91]

Figure 7 shows CLSM images of L/D-stained biofilms of *P. aeruginosa* reference strains (PAO1, PA14, RP73, and NH57388A) after overnight incubation with different SLN formulations in the LB medium.

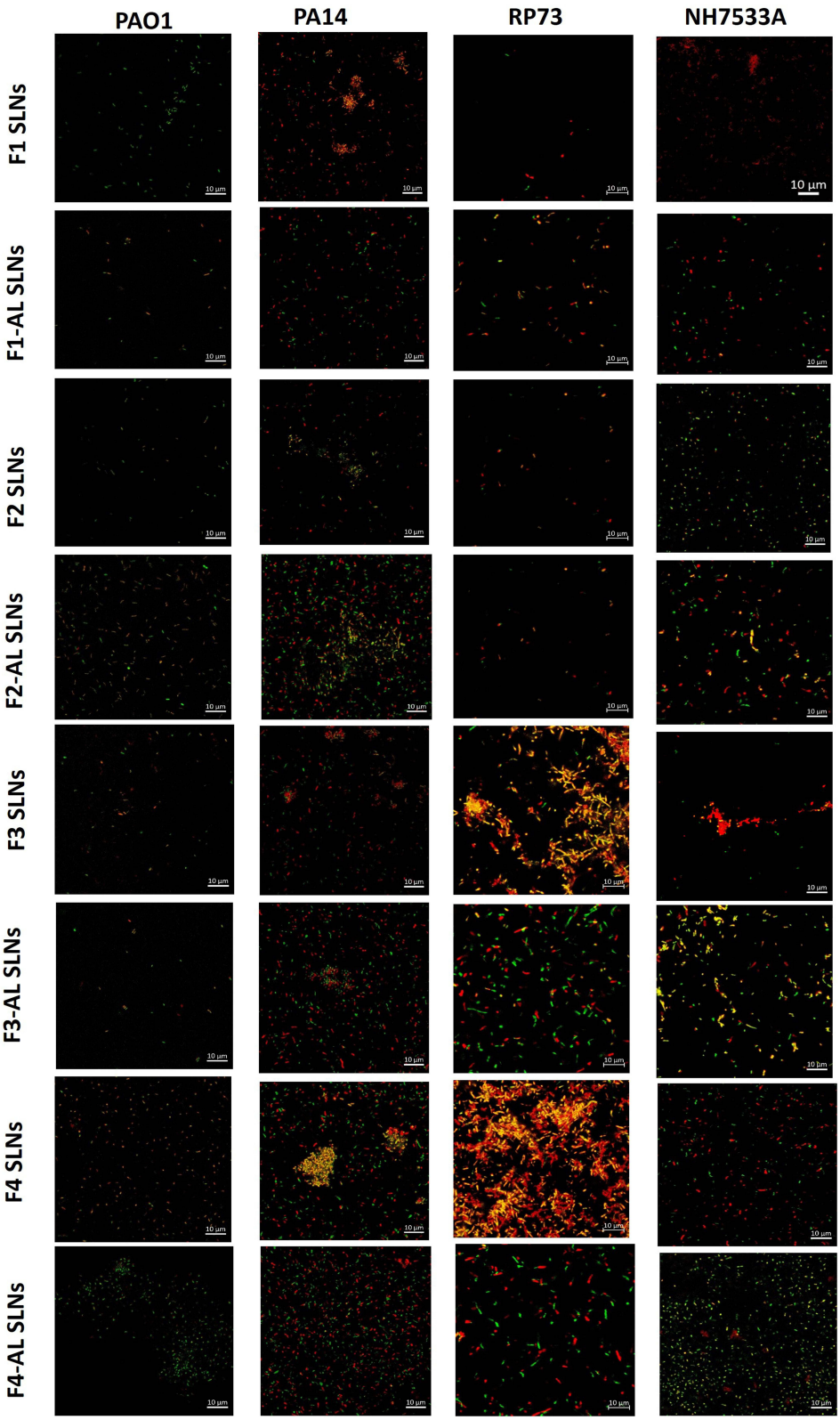

Figure 7 CLSM micrographs of *P. aeruginosa* biofilms of PA01, PA14, RP37, and NH57388A strains following exposure to different SLNs (Live/Dead staining).

CLSM images of PAO1 biofilms generally showed very weak fluorescence, suggesting efficient biofilm eradication, particularly in those exposed to F1-AL, F2, F3 and F3-AL SLNs. A remarkable density of live (green) *P. aeruginosa* was identified in F1 and F4-AL SLNs, whereas more dead (red) cells were observed in the case of chitosan-based F2 and F4

SLNs. Chitosan has been reported to cause a remarkable decrease in acyl homoserine lactone and pyocyanin production and motility in *P. aeruginosa*. CS and CS/ZnO nanocomposites downregulated the expression of L*as*I and *Rhl*I genes.[87]

A pronounced lethal potential was observed after treatment of the PA14 biofilm with F1, F3, and F4 SLNs, where red patches of dead pseudomonal microcolonies were observed. These clusters were absent in biofilms treated with AL-immobilized SLNs, revealing a more homogeneous distribution together with extensive proportions of live/dead cells (Figure 7).

Negatively charged particles seemingly demonstrated the biofilm eradication efficacy of RP73, showing minor green fluorescence (denoting live bacteria). In comparison, almost equal proportions of L/D bacteria were recognized with AL-immobilized CS-coated SLNs (F3-AL and F4-AL SLNs). Interestingly, RP73 biofilms treated with F3 and F4 SLNs exhibited a large colonization pattern, namely dead bacteria (Figure 7). Analogous behavior was observed in the NH57388A biofilms. CLSM micrographs of the NH57388A biofilms showed the highest proportion of live bacteria after exposure to F2 and F4-AL SLNs. Cotton et al[5] concluded that coadministration of gentamicin (1.0 µg/mL) with AL (20 units/mL) resulted in a 3000-fold reduction in bacterial concentration in established *P. aeruginosa* biofilms, which was significantly augmented with ciprofloxacin.

As stated by Rozenbaum,[72] CLSM images of *P. aeruginosa* ATCC 39324 biofilms grown with ASM showed a heterogeneous distribution of microcolonies surrounded by microchannels, whereas those grown with LB had a highly homogeneous structure without microcolonies and less obvious microchannels. Polysaccharides and eDNA in ASM-grown biofilms act as glue in the biofilm matrix, resulting in more compact biofilms. However, the culture medium had an insignificant effect on biofilm thickness and biovolume.[72]

Effect of SLNs on Extracellular Biofilm Matrix

As the developed system was designed mainly to target the extracellular matrix, calcofluor was used to stain extracellular polysaccharides and monitor biofilm density after exposure to SLNs. Being a polysaccharide, chitosan (in CS-modified SLNs) would be liable for interaction as well. An important limitation of the method is the ability of calcofluor to stain chitosan (a polysaccharide) which would make it harder to ascertain how much of the blue stained areas represent chitosan containing SLNs and which represent extracellular biofilm polysaccharide.

Z-stacks (Figure 8) generally reveal live bacteria (green) embedded in the extracellular matrix (blue). Interruption of the mature biofilm was obvious in the PAO1 strain incubated with anionic SLNs, especially AL-immobilized species, where live bacteria could be scarcely noticed, and the blue extracellular polysaccharide was repressed. The occurrence of dark areas reveals the existence of water channels.[92] Alginate lyases degrade alginate via beta-elimination of the glycosidic bond yielding various oligosaccharides with unsaturated uronic acid at the nonreducing terminus and unsaturated uronic acid monomers.[6] The putative catalytic mechanism of AL involves, first, the neutralization of the carboxyl negative charge by Arg and Asn, followed by abstracting the proton on C5 by a catalytic residue such as Tyr via general base catalysis. The resulting carboxylate dianion is then stabilized by His, resulting in proton donation from Tyr to form a double bond between C4 and C5, and cleavage of the glycosidic bond.[6]

In contrast, incubation of PAO1 with F3 and F4 SLNs elicited an overwhelming blue stain that could be reflecting either the dense biofilm matrix encasing the microcolonies or the abundant distribution of CS-SLNs (related to CS-calcofluor interaction) or both.

Analogous to PAO1, particle impact on the biofilm matrix was observed in the case of the RP73 strain (Figure 8). Interestingly, a relatively higher proportion of live bacteria (green) remained abundant in all stacks; this would be a privilege as the QSI used is intended to exert an anti-virulence rather than bactericidal action that ends up with rigorous microbial resistance.

The effect of SLNs on the biofilm matrix was less pronounced in the case of PA14. The blue network of the extracellular matrix generally concurs regardless of the particle type. Biofilms treated with F1-AL and F3-AL SLNs were less compact, with evident microchannels (Figure 8). Those treated with the F2-AL, F4, and F4-AL SLNs showed ample blue revealing either biofilm-embedded bacterial microcolonies serving as substrate/niche for new pathogens or CS-SLNs bound to bacterial walls. Calcofluor complex with chitosan was reported to visualize the interaction of chitosan with microbial cell wall in recent studies.[27,93,94]

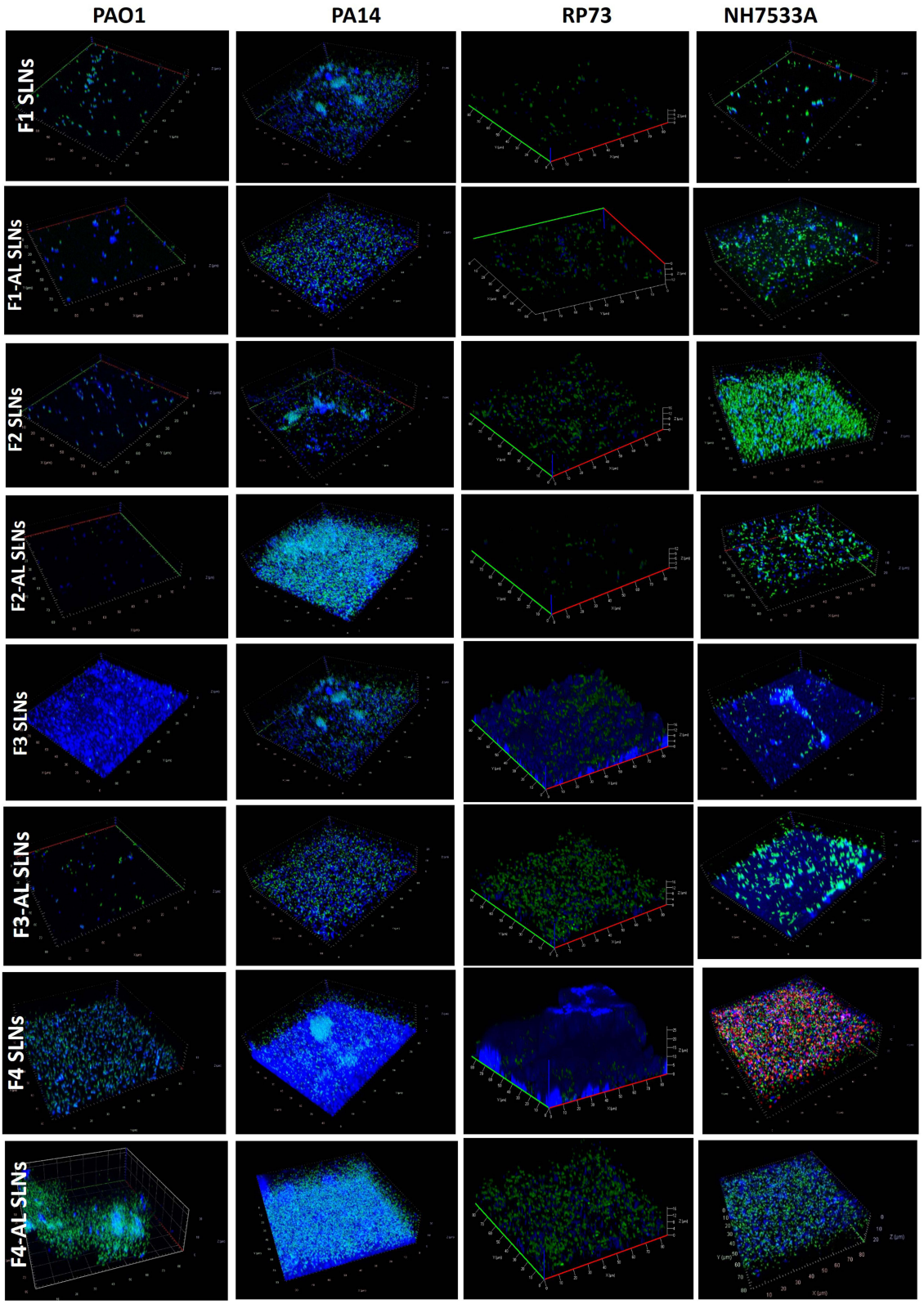

Figure 8 3D-time laps stacks (80 × 80×20 μm) of *P. aeruginosa* biofilms of PA01, PA14, RP37, and NH57388A strains showing live bacteria (stained green with Syto-9) and extracellular polysaccharides (stained blue with Calcofluor) following exposure to different SLNs.

In case of NH57388A, superior eradication of biofilms was realized by F1, F1-AL and F2 SLNs. Live pseudomonal microcolonies can also be observed. The interaction between calcofluor and chitosan in CS-coated SLNs is still to be noted. In spite of the ability of AL to depolymerize alginate, the incidence of calcium and zinc cations in CF lung was found to quench the enzyme activity via formation of recalcitrant alginate-cation complexes.[88] The presence of Ca^{2+} (1 mM Ca^{2+}) in the growth medium of the mucoid biofilm of *P. aeruginosa* environmental strain SG81 defines the biofilm architecture. Ca^{2+} stabilizes the cross-bridges between alginate molecules, allowing the formation of a thicker and more stable biofilm.[2] According to Germoni et al,[88] neither the biomass of *P. aeruginosa* biofilms nor their sensitivity to gentamicin was significantly affected by the AL enzyme when grown in liquid medium despite its obvious effect on biofilm morphology.

Z-stacks represent visual evidence consistent with data obtained by OD measurements elaborated in Figure 5.

Several indirect methods have been reported for measuring biofilm biomass. OD-based techniques allow for rapid screening of the overall mass, yet the multi-well plate reader cannot provide spatially resolved data.[92] Alternatively, SEM/TEM microscopy usually necessitates dehydration, thus enabling visualization of remnants of the original biofilm structure.[92] CLSM with double staining, hence preserving the biofilm structure, represents a superior technique.

The loud dogma of CS antimicrobial activity was related to the electrostatic interaction of CS with lipopolysaccharides (Gram negative bacteria) or teichoic acid (Gram positive bacteria). The presented data highlight the undeniable complex influence of chitosan on biofilms, which represents a paradigm shift.

Uptake of SLNs in P. aeruginosa Biofilm

The established *P. aeruginosa* biofilms were stained (red) with propidium iodide following incubation with coumarin-labeled SLNs (green) to investigate the binding and uptake behavior of the developed nanocarriers with bacteria. CLSM images (Figure 9) showed clear colocalization of SLNs in the vicinity of bacterial cells, particularly in the case of the cou-F1 SLNs with RP73 biofilms. While red-stained cells denote dead bacteria, staining live candidates with SYTO-9 was not convenient because of the overlap with the green fluorescence of coumarin 6. Nevertheless, spots of labeled SLNs could be recognized in the micrographs (as indicated by arrows) seemingly attached to viable unstained bacterial cells (Figure 9), in particular, the cou-F3 and cou-F3-AL SLNs with PA14 biofilms. A lower extent of particle uptake could be achieved in the case of mucoid NH57388A biofilms and was difficult to follow in the case of PAO1 biofilms (data not shown).

When discussing SLN uptake in bacteria, exploring particle–membrane interaction is imperative. On top is the interaction of chitosan with LPS glycolipids in the outer cell membrane of *P. aeruginosa*, whereby, forces other than electrostatic interactions may contribute to complex formation.[95] In the current study, we used LMW-CS (20 kDa), which was reported for higher affinity for LPS relative to HMW-CS (140 kDa).[95]

Conclusions

The alginate lyase enzyme, recently elected for developing alginate-degrading CF biotherapies, was immobilized on the surface of the SLNs. Anionic SLNs were loaded with an early stage alkylquinolone-based quorum-sensing inhibitor that disrupted bacterial cell-to-cell communication and were coated with chitosan to obtain cationic SLNs. The particles ensured good penetrability across the artificial sputum-biofilm model and adequate viability and uptake in human bronchial and alveolar cell lines. With an eye toward therapeutic applications, inhalable microparticles were prepared to elicit the appropriate aerodynamic parameters. Antipseudomonal activity was verified in four *P. aeruginosa* reference strains and five clinical isolates via OD measurements, Live/Dead staining and CLSM 3D-time lapse imaging. SLNs showed the potential for growth inhibition of planktonically grown bacteria, antibiofilm, and biofilm eradication efficacy as a function of the bacterial strain, growth medium, particle composition, payload, and concentration. Confocal z-stacks of the stained extracellular matrix highlighted the effect of AL on biofilm disruption; however, chitosan-coated SLNs promoted the establishment of overwhelming biofilms. Uptake experiments illustrated labeled SLNs in the vicinity of biofilm colonies. Notably, the improved and structure-divergent QSI outperformed the chemical class used in this study in terms of potency. These new chemical entities provide the basis for the further functionalization of intricate NP-based systems. Taken together, the study emphasizes that the taboo "nanocarriers are inert" no longer applies. Accordingly, thorough tailoring of formulated nanocarriers is recommended to prevent cross-linking with polyanionic components

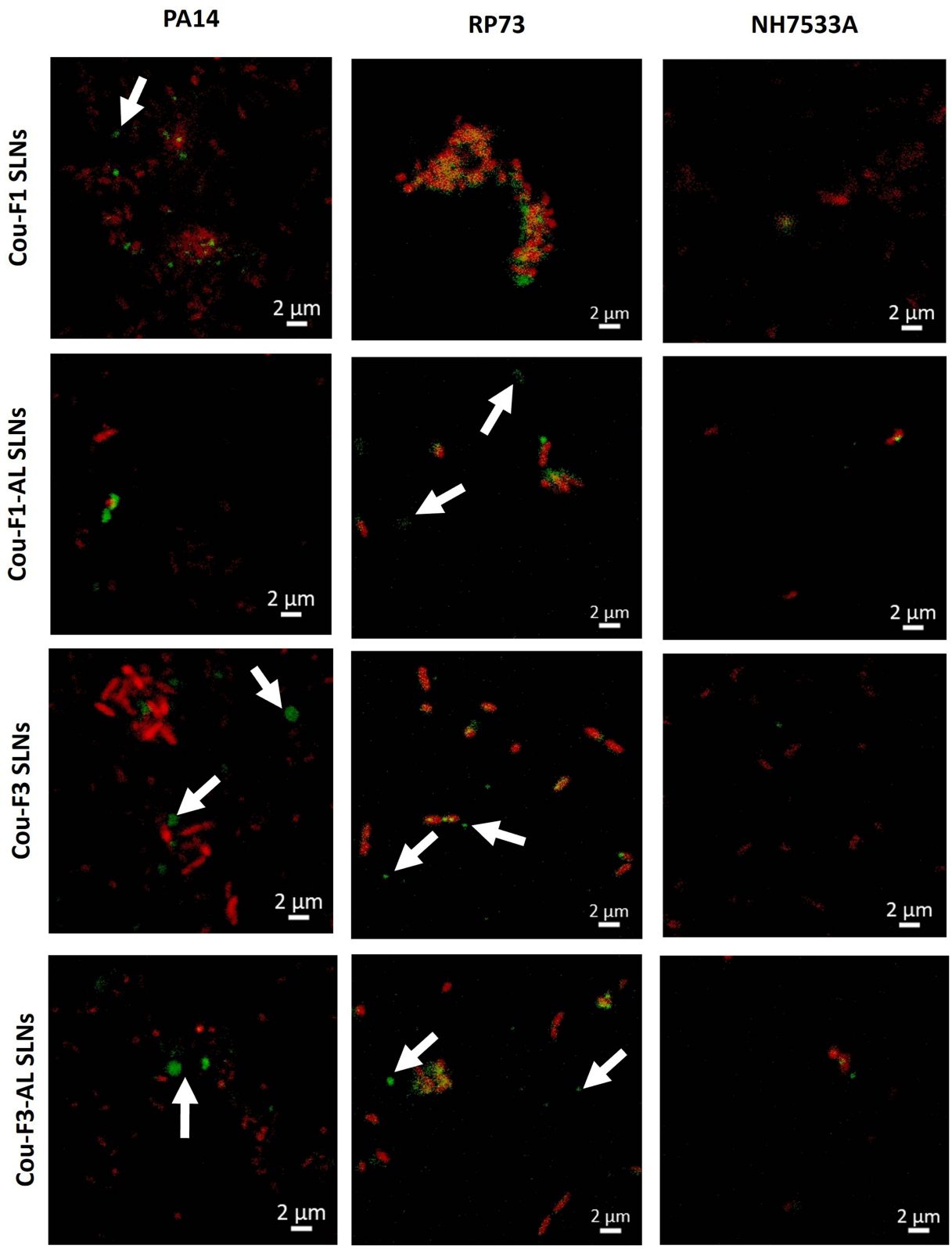

Figure 9 Uptake of coumarin-labeled SLNs (green) in PA14, RP37, and NH57388A strains (dead bacteria stained red). Arrows represent SLN clusters around live non-stained bacteria. Scale bar 2 µm.

(DNA, F-actin, lipopolysaccharide, and lipoteichoic acid) in the sputum/biofilm barrier to smoothly penetrate the EPS biofilm matrix.

Acknowledgments

Authors acknowledge the Alexander von Humboldt Foundation, Germany for funding this research under The Research Group Linkage Programme.

Disclosure

Martin Empting reports a patent WO2020007938A1 pending to Helmholtz Centre for Infection Research (HZI), a patent EP20150104 pending to Helmholtz Centre for Infection Research (HZI), and a patent WO2021136805A1 pending to Helmholtz Centre for Infection Research (HZI). The authors report no other conflicts of interest in this work.

References

1. Malhotra S, Hayes D, Wozniak Daniel J. Cystic fibrosis and pseudomonas aeruginosa: the host-microbe interface. *Clin Microbiol Rev*. 2019;32(3): e00138–00118. doi:10.1128/CMR.00138-18
2. Flemming H-C, Wingender J. The biofilm matrix. *Nat Rev Microbiol*. 2010;8(9):623–633. doi:10.1038/nrmicro2415
3. Hadinoto K, Cheow WS. Nano-antibiotics in chronic lung infection therapy against Pseudomonas aeruginosa. *Colloids Surf B*. 2014;116:772–785. doi:10.1016/j.colsurfb.2014.02.032
4. Maunders E, Welch M. Matrix exopolysaccharides; the sticky side of biofilm formation. *FEMS Microbiol Lett*. 2017;364(13). doi:10.1093/femsle/fnx120
5. Cotton LA, Graham RJ, Lee RJ. The role of alginate in P. aeruginosa PAO1 biofilm structural resistance to gentamicin and ciprofloxacin. *J Exp Microbiol Immunol*. 2009;13:58–62.
6. Kim HS, Lee C-G, Lee EY. Alginate lyase: structure, property, and application. *Biotechnol Bioprocess Eng*. 2011;16(5):843. doi:10.1007/s12257-011-0352-8
7. Omri A, Beaulac C, Bouhajib M, Montplaisir S, Sharkawi M, Lagace J. Pulmonary retention of free and liposome-encapsulated tobramycin after intratracheal administration in uninfected rats and rats infected with Pseudomonas aeruginosa. *Antimicrob Agents Chemother*. 1994;38(5):1090–1095. doi:10.1128/AAC.38.5.1090
8. Patel KK, Tripathi M, Pandey N, et al. Alginate lyase immobilized chitosan nanoparticles of ciprofloxacin for the improved antimicrobial activity against the biofilm associated mucoid P. aeruginosa infection in cystic fibrosis. *Int J Pharm*. 2019;563:30–42. doi:10.1016/j.ijpharm.2019.03.051
9. Li S, Wang Y, Li X, Lee BS, Jung S, Lee M-S. Enhancing the thermo-stability and anti-biofilm activity of alginate lyase by immobilization on low molecular weight chitosan nanoparticles. *Int J Mol Sci*. 2019;20(18):4565. doi:10.3390/ijms20184565
10. Günday Türeli N, Torge A, Juntke J, et al. Ciprofloxacin-loaded PLGA nanoparticles against cystic fibrosis P. aeruginosa lung infections. *Eur J Pharm Biopharm*. 2017;117:363–371. doi:10.1016/j.ejpb.2017.04.032
11. Torge A, Wagner S, Chaves PS, et al. Ciprofloxacin-loaded lipid-core nanocapsules as mucus penetrating drug delivery system intended for the treatment of bacterial infections in cystic fibrosis. *Int J Pharm*. 2017;527(1–2):92–102. doi:10.1016/j.ijpharm.2017.05.013
12. Gunday Tureli N, Tureli AE, Schneider M. Inhalable antibiotic nanoformulations for the treatment of pseudomonas aeruginosa infection in cystic fibrosis – a review. *Drug Deliv Lett*. 2014;4(3):193–207. doi:10.2174/2210303104666140222002101
13. Alipour M, Suntres ZE, Omri A. Importance of DNase and alginate lyase for enhancing free and liposome encapsulated aminoglycoside activity against Pseudomonas aeruginosa. *J Antimicrob Chemother*. 2009;64(2):317–325. doi:10.1093/jac/dkp165
14. Chemani C, Imberty A, de Bentzmann S, et al. Role of LecA and LecB Lectins in Pseudomonas aeruginosa-induced lung injury and effect of carbohydrate ligands. *Infect Immun*. 2009;77(5):2065–2075. doi:10.1128/IAI.01204-08
15. Baelo A, Levato R, Julián E, et al. Disassembling bacterial extracellular matrix with DNase-coated nanoparticles to enhance antibiotic delivery in biofilm infections. *J Control Release*. 2015;209:150–158. doi:10.1016/j.jconrel.2015.04.028
16. Hurley MN, Cámara M, Smyth AR. Novel approaches to the treatment of Pseudomonas aeruginosa infections in cystic fibrosis. *Eur Respir J*. 2012;40(4):1014. doi:10.1183/09031936.00042012
17. Reymond J-L, Bergmann M, Darbre T. Glycopeptide dendrimers as Pseudomonas aeruginosa biofilm inhibitors. *Chem Soc Rev*. 2013;42 (11):4814–4822. doi:10.1039/c3cs35504g
18. Hamed MM, Abdelsamie AS, Rox K, et al. Towards translation of PqsR inverse agonists: from in vitro efficacy optimization to in vivo proof-of-principle. *Adv Sci*. 2023;10(5):2204443. doi:10.1002/advs.202204443
19. Wagner S, Sommer R, Hinsberger S, et al. Novel strategies for the treatment of pseudomonas aeruginosa infections. *J Med Chem*. 2016;59 (13):5929–5969. doi:10.1021/acs.jmedchem.5b01698
20. Hartmann R, Steinbach A, Lu C, et al. Helmholtz-Zentrums für Infektionsforschung, Braunschweig, assignee. PqsR modulators; 2014.
21. Lu C, Kirsch B, Maurer CK, et al. Optimization of anti-virulence PqsR antagonists regarding aqueous solubility and biological properties resulting in new insights in structure–activity relationships. *Eur J Med Chem*. 2014;79:173–183. doi:10.1016/j.ejmech.2014.04.016
22. Lu C, Kirsch B, Zimmer C, et al. Discovery of antagonists of PqsR, a key player in 2-alkyl-4-quinolone-dependent quorum sensing in *Pseudomonas aeroginosae*. *Chem Biol*. 2012;19(3):381–390. doi:10.1016/j.chembiol.2012.01.015
23. Lu C, Maurer CK, Kirsch B, Steinbach A, Hartmann RW. Overcoming the unexpected functional inversion of a PqsR antagonist in Pseudomonas aeruginosa: an in vivo potent antivirulence agent targeting pqs quorum sensing. *Angewandte Chemie*. 2014;53(4):1109–1112. doi:10.1002/anie.201307547
24. Schütz C, D-K H, Hamed MM, et al. A new PqsR inverse agonist potentiates tobramycin efficacy to eradicate pseudomonas aeruginosa biofilms. *Adv Sci*. 2021;8(12):2004369. doi:10.1002/advs.202004369

25. Schütz C, Hodzic A, Hamed M, et al. Divergent synthesis and biological evaluation of 2-(trifluoromethyl)pyridines as virulence-attenuating inverse agonists targeting PqsR. *Eur J Med Chem*. 2021;226:113797. doi:10.1016/j.ejmech.2021.113797
26. Nafee N, Husari A, Maurer CK, et al. Antibiotic-free nanotherapeutics: ultra-small, mucus-penetrating solid lipid nanoparticles enhance the pulmonary delivery and anti-virulence efficacy of novel quorum sensing inhibitors. *J Control Release*. 2014;192:131–140. doi:10.1016/j.jconrel.2014.06.055
27. Marangon CA, Martins VCA, Ling MH, et al. Combination of rhamnolipid and chitosan in nanoparticles boosts their antimicrobial efficacy. *ACS Appl Mater Interfaces*. 2020;12(5):5488–5499. doi:10.1021/acsami.9b19253
28. Alkawash MA, Soothill JS, Schiller NL. Alginate lyase enhances antibiotic killing of mucoid Pseudomonas aeruginosa in biofilms. *Apmis*. 2006;114(2):131–138. doi:10.1111/j.1600-0463.2006.apm_356.x
29. Yang M, Yang SX, Liu ZM, Li NN, Li L, Mou HJ. Rational Design of alginate lyase from microbulbifer sp. Q7 to improve thermal stability. *Mar Drugs*. 2019;17(6):378. doi:10.3390/md17060378
30. Yang M, Yu Y, Yang S, Shi X, Mou H, Li L. Expression and characterization of a New PolyG-specific alginate lyase from marine bacterium microbulbifer sp. Q7. *Front Microbiol*. 2018;9:2894. doi:10.3389/fmicb.2018.02894
31. Wan B, Zhu Y, Tao J, et al. Alginate lyase guided silver nanocomposites for eradicating Pseudomonas aeruginosa from lungs. *ACS Appl Mater Interfaces*. 2020;12(8):9050–9061. doi:10.1021/acsami.9b21815
32. Kamal AAM, Petrera L, Eberhard J, Hartmann RW. Structure–functionality relationship and pharmacological profiles of Pseudomonas aeruginosa alkylquinolone quorum sensing modulators. *Org Biomol Chem*. 2017;15(21):4620–4630. doi:10.1039/C7OB00263G
33. Shi C, Ahmad Khan S, Wang K, Schneider M. Improved delivery of the natural anticancer drug tetrandrine. *Int J Pharm*. 2015;479(1):41–51. doi:10.1016/j.ijpharm.2014.12.022
34. Kirchner S, Fothergill JL, Wright EA, James CE, Mowat E, Winstanley C. Use of artificial sputum medium to test antibiotic efficacy against Pseudomonas aeruginosa in conditions more relevant to the cystic fibrosis lung. *J Visualized Exp*. 2012;64:e3857.
35. Nafee N, Forier K, Braeckmans K, Schneider M. Mucus-penetrating solid lipid nanoparticles for the treatment of cystic fibrosis: proof of concept, challenges and pitfalls. *Eur J Pharm Biopharm*. 2018;124:125–137. doi:10.1016/j.ejpb.2017.12.017
36. Friedl H, Dünnhaupt S, Hintzen F, et al. Development and evaluation of a novel mucus diffusion test system approved by self-nanoemulsifying drug delivery systems. *J Pharmaceut Sci*. 2013;102(12):4406–4413. doi:10.1002/jps.23757
37. Stöber W. A note on the aerodynamic diameter and the mobility of non-spherical aerosol particles. *J Aerosol Sci*. 1971;2(4):453–456. doi:10.1016/0021-8502(71)90048-6
38. Makled S, Boraie N, Nafee N. Nanoparticle-mediated macrophage targeting—a new inhalation therapy tackling tuberculosis. *Drug Delivery Transl Res*. 2021;11(3):1037–1055. doi:10.1007/s13346-020-00815-3
39. Song Y, Salinas D, Nielson DW, Verkman AS. Hyperacidity of secreted fluid from submucosal glands in early cystic fibrosis. *Am J Physiol Cell Physiol*. 2006;290(3):C741–C749. doi:10.1152/ajpcell.00379.2005
40. Gordillo-Galeano A, Mora-Huertas CE. Solid lipid nanoparticles and nanostructured lipid carriers: a review emphasizing on particle structure and drug release. *Eur J Pharm Biopharm*. 2018;133:285–308. doi:10.1016/j.ejpb.2018.10.017
41. Mohapatra BR. Biocatalytic characteristics of chitosan nanoparticle-immobilized alginate lyase extracted from a novel Arthrobacter species AD-10. *Biocatal Agric Biotechnol*. 2020;23:101458. doi:10.1016/j.bcab.2019.101458
42. Panigrahi KC, Patra CN, Jena GK, et al. Gelucire: a versatile polymer for modified release drug delivery system. *Future J Pharm Sci*. 2018;4(1):102–108. doi:10.1016/j.fjps.2017.11.001
43. Popat A, Liu J, Lu GQ, Qiao SZ. A pH-responsive drug delivery system based on chitosan coated mesoporous silica nanoparticles. *J Mater Chem*. 2012;22(22):11173–11178. doi:10.1039/c2jm30501a
44. Chronopoulou L, Massimi M, Giardi MF, et al. Chitosan-coated PLGA nanoparticles: a sustained drug release strategy for cell cultures. *Colloids Surf B*. 2013;103:310–317. doi:10.1016/j.colsurfb.2012.10.063
45. Mazzarino L, Borsali R, Lemos-Senna E. Mucoadhesive films containing chitosan-coated nanoparticles: a new strategy for buccal curcumin release. *J Pharmaceut Sci*. 2014;103(11):3764–3771. doi:10.1002/jps.24142
46. Mehnert W, Mäder K. Solid lipid nanoparticles: production, characterization and applications. *Adv Drug Delivery Rev*. 2001;47(2–3):165–196. doi:10.1016/S0169-409X(01)00105-3
47. Dumortier G, Grossiord JL, Agnely F, Chaumeil JC. A review of poloxamer 407 pharmaceutical and pharmacological characteristics. *Pharm Res*. 2006;23(12):2709–2728. doi:10.1007/s11095-006-9104-4
48. Si L, Yang S, Lin R, Gu S, Yan C, Yan J. SiO2–alginate–melittin nano-conjugates suppress the proliferation of ovarian cancer cells: a controlled release approach leveraging alginate lyase. *Cancer Nanotechnol*. 2024;15(1):4. doi:10.1186/s12645-023-00241-3
49. Nafee N, Taetz S, Schneider M, Schaefer UF, Lehr CM. Chitosan-coated PLGA nanoparticles for DNA/RNA delivery: effect of the formulation parameters on complexation and transfection of antisense oligonucleotides. *Nanomedicine*. 2007;3(3):173–183. doi:10.1016/j.nano.2007.03.006
50. Taetz S, Nafee N, Beisner J, et al. The influence of chitosan content in cationic chitosan/PLGA nanoparticles on the delivery efficiency of antisense 2'-O-methyl-RNA directed against telomerase in lung cancer cells. *Eur J Pharm Biopharm*. 2009;72(2):358–369. doi:10.1016/j.ejpb.2008.07.011
51. Huck BC, Hartwig O, Biehl A, et al. Macro- and microrheological properties of mucus surrogates in comparison to native intestinal and pulmonary mucus. *Biomacromolecules*. 2019;20(9):3504–3512. doi:10.1021/acs.biomac.9b00780
52. Pritchard Manon F, Powell Lydia C, Jack Alison A, et al. A low-molecular-weight alginate oligosaccharide disrupts pseudomonal microcolony formation and enhances antibiotic effectiveness. *Antimicrob Agents Chemother*. 2017;61(9):e00762–00717. doi:10.1128/AAC.00762-17
53. Finke JH, Richter C, Gothsch T, Kwade A, Büttgenbach S, Müller-Goymann CC. Coumarin 6 as a fluorescent model drug: how to identify properties of lipid colloidal drug delivery systems via fluorescence spectroscopy? *Eur J Lipid Sci Technol*. 2014;116(9):1234–1246. doi:10.1002/ejlt.201300413
54. Suk JS, Lai SK, Wang -Y-Y, et al. The penetration of fresh undiluted sputum expectorated by cystic fibrosis patients by non-adhesive polymer nanoparticles. *Biomaterials*. 2009;30(13):2591–2597. doi:10.1016/j.biomaterials.2008.12.076
55. Schlafer S, Meyer RL. Confocal microscopy imaging of the biofilm matrix. *J Microbiol Methods*. 2017;138:50–59. doi:10.1016/j.mimet.2016.03.002
56. Strathmann M, Wingender J, Flemming H-C. Application of fluorescently labelled lectins for the visualization and biochemical characterization of polysaccharides in biofilms of Pseudomonas aeruginosa. *J Microbiol Methods*. 2002;50(3):237–248. doi:10.1016/S0167-7012(02)00032-5
57. Messiaen AS, Forier K, Nelis H, Braeckmans K, Coenye T, Kaufmann GF. Transport of nanoparticles and tobramycin-loaded liposomes in Burkholderia cepacia complex biofilms. *PLoS One*. 2013;8(11):e79220. doi:10.1371/journal.pone.0079220

58. Ungaro F, d'Angelo I, Coletta C, et al. Dry powders based on PLGA nanoparticles for pulmonary delivery of antibiotics: modulation of encapsulation efficiency, release rate and lung deposition pattern by hydrophilic polymers. *J Control Release*. 2012;157(1):149–159. doi:10.1016/j.jconrel.2011.08.010
59. Tan Y, Ma S, Leonhard M, et al. Enhancing antibiofilm activity with functional chitosan nanoparticles targeting biofilm cells and biofilm matrix. *Carbohydr Polym*. 2018;200:35–42. doi:10.1016/j.carbpol.2018.07.072
60. Patel KK, Agrawal AK, Anjum MM, et al. DNase-I functionalization of ciprofloxacin-loaded chitosan nanoparticles overcomes the biofilm-mediated resistance of Pseudomonas aeruginosa. *Appl Nanosci*. 2020;10(2):563–575. doi:10.1007/s13204-019-01129-8
61. Nafee N, Gaber DM, Elzoghby AO, Helmy MW, Abdallah OY. Promoted antitumor activity of myricetin against lung carcinoma via nanoencapsulated phospholipid complex in respirable microparticles. *Pharm Res*. 2020;37(4):82. doi:10.1007/s11095-020-02794-z
62. Grace A, Sahu R, Owen DR, Dennis VA. Pseudomonas aeruginosa reference strains PAO1 and PA14: a genomic, phenotypic, and therapeutic review. *Front Microbiol*. 2022;13:1023523.
63. DeNegre AA, Myers K, Fefferman NH. Impact of strain competition on bacterial resistance in immunocompromised populations. *Antibiotics*. 2020;9(3):114. doi:10.3390/antibiotics9030114
64. Chandler Courtney E, Horspool Alexander M, Hill Preston J, et al. Genomic and phenotypic diversity among ten laboratory isolates of Pseudomonas aeruginosa PAO1. *J Bacteriol*. 2019;201(5). doi:10.1128/jb.00595-00518
65. Mikkelsen H, McMullan R, Filloux A, Cornelis P. The Pseudomonas aeruginosa reference strain PA14 displays increased virulence due to a mutation in ladS. *PLoS One*. 2011;6(12):e29113–e29113. doi:10.1371/journal.pone.0029113
66. Sana TG, Lomas R, Gimenez MR, et al. Differential modulation of quorum sensing signaling through QslA in Pseudomonas aeruginosa Strains PAO1 and PA14. *J Bacteriol*. 2019;201(21). doi:10.1128/jb.00362-00319
67. Liu Y, Ahator SD, Wang H, et al. Microevolution of the mexT and lasR reinforces the bias of quorum sensing system in laboratory strains of Pseudomonas aeruginosa PAO1. *Front Microbiol*. 2022;13:821895.
68. Luria-Bertani LB. Liquid medium. *Cold Spring Harbor Protocols*. 2006;2006(1):pdb.rec8141.
69. Korgaonkar AK, Whiteley M. Pseudomonas aeruginosa enhances production of an antimicrobial in response to N-acetylglucosamine and peptidoglycan. *J Bacteriol*. 2011;193(4):909–917. doi:10.1128/JB.01175-10
70. Neve Rachel L, Carrillo Brent D, Phelan Vanessa V. Impact of artificial sputum medium formulation on Pseudomonas aeruginosa secondary metabolite production. *J Bacteriol*. 2021;203(21):e00250–00221. doi:10.1128/JB.00250-21
71. Matilla Miguel A, Martín-Mora D, Gavira Jose A, Krell T. Pseudomonas aeruginosa as a model to study chemosensory pathway signaling. *Microbiol Mol Biol Rev*. 2021;85(1). doi:10.1128/mmbr.00151-00120
72. Rozenbaum R Antimicrobial and nanoparticle penetration and killing in infectious biofilms. Groningen, Rijksuniversiteit Groningen; 2019.
73. Reighard KP, Hill DB, Dixon GA, Worley BV, Schoenfisch MH. Disruption and eradication of P. aeruginosa biofilms using nitric oxide-releasing chitosan oligosaccharides. *Biofouling*. 2015;31(9–10):775–787. doi:10.1080/08927014.2015.1107548
74. Gimmestad M, Sletta H, Ertesvåg H, et al. The Pseudomonas fluorescens AlgG Protein, but not its mannuronan C-5-epimerase activity, is needed for alginate polymer formation. *J Bacteriol*. 2003;185(12):3515–3523. doi:10.1128/JB.185.12.3515-3523.2003
75. Russell NJ, Gacesa P. Chemistry and biology of the alginate of mucoid strains of Pseudomonas aeruginosa in cystic fibrosis. *Mol Aspect Med*. 1988;10(1):1–91. doi:10.1016/0098-2997(88)90002-7
76. Boyd A, Chakrabarty AM. Role of alginate lyase in cell detachment of Pseudomonas aeruginosa. *Appl Environ Microbiol*. 1994;60(7):2355–2359. doi:10.1128/aem.60.7.2355-2359.1994
77. Lamppa JW, Griswold KE. Alginate lyase exhibits catalysis-independent biofilm dispersion and antibiotic synergy. *Antimicrob Agents Chemother*. 2013;57(1):137–145. doi:10.1128/AAC.01789-12
78. Meers P, Neville M, Malinin V, et al. Biofilm penetration, triggered release and in vivo activity of inhaled liposomal amikacin in chronic Pseudomonas aeruginosa lung infections. *J Antimicrob Chemother*. 2008;61(4):859–868. doi:10.1093/jac/dkn059
79. Alhajlan M, Alhariri M, Omri A. Efficacy and safety of liposomal clarithromycin and its effect on Pseudomonas aeruginosa virulence factors. *Antimicrob Agents Chemother*. 2013;57(6):2694–2704. doi:10.1128/AAC.00235-13
80. Drulis-Kawa Z, Gubernator J, Dorotkiewicz-Jach A, Doroszkiewicz W, Kozubek A. In vitro antimicrobial activity of liposomal meropenem against Pseudomonas aeruginosa strains. *Int J Pharm*. 2006;315(1–2):59–66. doi:10.1016/j.ijpharm.2006.02.017
81. Jesus S, Schmutz M, Som C, Borchard G, Wick P, Borges O. Hazard assessment of polymeric nanobiomaterials for drug delivery: what can we learn from literature so far. *Front Bioeng Biotechnol*. 2019;7:261. doi:10.3389/fbioe.2019.00261
82. Yermak IM, Davidova VN, Gorbach VI, et al. Forming and immunological properties of some lipopolysaccharide–chitosan complexes. *Biochimie*. 2006;88(1):23–30. doi:10.1016/j.biochi.2005.07.004
83. Yamada H, Koike N, Ehara T, Matsumoto T. Measuring antimicrobial susceptibility of Pseudomonas aeruginosa using Poloxamer 407 gel. *J Infect Chemother*. 2011;17(2):195–199. doi:10.1007/s10156-010-0109-x
84. Taylor BJ, Marsh LL, Nosworthy JO, Williams DW. A novel approach to antibiofilm susceptibility testing using a thermo-reversible matrix. *J Wound Care*. 2016;25(2):62–67. doi:10.12968/jowc.2016.25.2.62
85. Bose SK, Nirbhavane P, Batra M, Chhibber S, Harjai K. Nanolipoidal α-terpineol modulates quorum sensing regulated virulence and biofilm formation in Pseudomonas aeruginosa. *Nanomedicine*. 2020;15(18):1743–1760. doi:10.2217/nnm-2020-0134
86. Cheow WS, Chang M, Hadinoto K. The roles of lipid in anti-biofilm efficacy of lipid-polymer hybrid nanoparticles encapsulating antibiotics. *Colloids Surf A*. 2011;389(1–3):158–165.
87. Badawy MSEM, Riad OKM, Taher FA, Zaki SA. Chitosan and chitosan-zinc oxide nanocomposite inhibit expression of LasI and RhlI genes and quorum sensing dependent virulence factors of Pseudomonas aeruginosa. *Int J Biol Macromol*. 2020;149:1109–1117. doi:10.1016/j.ijbiomac.2020.02.019
88. Germoni L, Bremer P, Lamont I. The effect of alginate lyase on the gentamicin resistance of Pseudomonas aeruginosa in mucoid biofilms. *J Appl Microbiol*. 2016;121(1):126–135. doi:10.1111/jam.13153
89. Rivera Aguayo P, Bruna Larenas T, Alarcón Godoy C, et al. Antimicrobial and antibiofilm capacity of chitosan nanoparticles against wild type strain of Pseudomonas sp. isolated from milk of cows diagnosed with bovine mastitis. *Antibiotics*. 2020;9(9):551. doi:10.3390/antibiotics9090551
90. Kragh KN, Alhede M, Kvich L, Bjarnsholt T. Into the well—A close look at the complex structures of a microtiter biofilm and the crystal violet assay. *Biofilm*. 2019;1:100006. doi:10.1016/j.bioflm.2019.100006

91. Quintas V, Prada-López I, Tomás I. *Analyzing the Oral Biofilm Using Fluorescence-Based Microscopy: What's in a Dye?* Formatex Research Center; 2014.
92. Méndez-Vilas ADJ. *Microscopy: Science, Technology, Applications and Education*. Badajoz: Formatex Research Center; 2010.
93. Rizzi Yanina S, Happel P, Lenz S, et al. Chitosan and chitin deacetylase activity are necessary for development and virulence of Ustilago *maydis*. *mBio*. 2021;12(2). doi:10.1128/mbio.03419-03420
94. Somashekar D, Joseph R. A new spectrophotometric method of assay for chitosanase based on calcofluor white dye binding. *Carbohydr Polym*. 1997;34(4):343–346. doi:10.1016/S0144-8617(97)00052-0
95. Davydova VN, Yermak IM, Gorbach VI, Krasikova IN, Solov'eva TF. Interaction of bacterial endotoxins with chitosan. Effect of endotoxin structure, chitosan molecular mass, and ionic strength of the solution on the formation of the complex. *Biochem Biokhimiia*. 2000;65(9):1082–1090.